PCP
PLANT & CELL PHYSIOLOGY

Special Issue - Regular Paper

Fine-tuned terpene synthase gene expression, functional promiscuity, and subcellular localization: implications for the evolution of complex floral volatile bouquet in *Caladenia* orchids

Fei Zhou[1,2], Ya-Nan Zhao[1], James Perkins[3], Haiyang Xu[2], Eran Pichersky[2], Rod Peakall[3,*] and Darren C. J. Wong[3,4,*]

[1]State Key Laboratory of Pharmaceutical Biotechnology, School of Life Sciences, Nanjing University, Nanjing 210023, China, [2]Department of Molecular, Cellular and Developmental Biology, University of Michigan, Ann Arbor, MI 48104, USA, [3]Ecology and Evolution, Research School of Biology, The Australian National University, Canberra, ACT 2600, Australia, [4]School of Agriculture, Food, and Wine, Waite Research Precinct, University of Adelaide, Adelaide, SA 5064, Australia

*Corresponding author: Darren CJ Wong, E-mails, darren.wong@anu.edu.au, wongdcj@gmail.com; Rod Peakall, E-mail, rod.peakall@anu.edu.au
Received 6 August 2024; Accepted 11 March 2025

Abstract

Chemically mediated floral volatile signals are crucial for pollinator attraction across angiosperms. However, beyond model plant systems, the molecular mechanisms underpinning their tissue-specific biosynthesis, regulation, and emission are still poorly understood. In this study of a food-deceptive insect-pollinated orchid (*Caladenia denticulata*), we elucidated the molecular basis of α-pinene biosynthesis—the major floral volatile emitted by this species and diverse lower abundance monoterpenes and sesquiterpenes. To achieve this, we combined comparative transcriptomics between active glandular trichome-rich sepal tips and labellum and non-active remaining flower tissues, floral volatile headspace profiling, phylogenetic analysis of a multigene family, and protein functional assays. We found (i) multiple branch points of the terpene synthase (TPS) biosynthetic pathway were highly expressed and coordinately upregulated in the active floral tissues compared to non-active ones, (ii) the monoterpene synthase CdTPS-b3 underpinning α-pinene biosynthesis and a *bona fide* promiscuous TPS CdTPS-b4 that may contribute to the diverse array of low-abundance mono- and sesquiterpenes found in its flowers, and (iii) dual localization (plastid and cytosol) of CdTPS-b3 and CdTPS-b4. Our findings highlight metabolic pathway specialization at multiple TPS pathway branch points supporting the biosynthesis and emission of α-pinene in *C. denticulata* flowers that are implicated in its generalist pollinator attraction. Furthermore, the complexity of diverse floral terpenes in *Caladenia* is likely mediated by finely tuned TPS gene expression, functional promiscuity, and subcellular localization. We predict that the combination of these three mechanisms underpin the evolution of multiple deceptive pollination strategies in *Caladenia*.

Keywords: Orchid; Pollination; Transcriptome; Terpenoids; Terpene synthase; Glandular trichome

Introduction

Many flowering plants have evolved diverse strategies to communicate with and attract animal pollinators. Compared to other plant families, unusual and/or highly specialized deceptive pollination strategies are particularly widespread in the hyperdiverse orchid lineage (Jersáková et al. 2006). Recent estimates suggest that up to half of all orchids (approximately 10–15 000 species) employ deceptive pollination strategies (Ackerman et al. 2023). The false advertisement of food resources (generalized food deception) by rewardless but brightly coloured food deceptive (FD) species is by far the most common deceptive pollination strategy (Schiestl and Johnson 2013, Dormont et al. 2019). Flowers of many deceptive orchids have evolved complex means to entice and then defraud their insect pollinators (Jersáková et al. 2006).

The typical floral visual and olfactory signals involved in this deception involve plant specialized metabolites (PSMs) (Perkins et al. 2023, Wong et al. 2023). In many plants including orchids, accumulation of PSM pigments, especially flavonoids (Liang et al. 2020, Zhang et al. 2020, Wong et al. 2024) and carotenoids (Liu et al. 2019, Li et al. 2020), confer the showy flower colours. Spatiotemporal regulation of pigments further underpins the intricate colour patterns (e.g. spots, blotches,

Plant And Cell Physiology, 2025, 66(4), 627–644
doi:https://doi.org/10.1093/pcp/pcaf026
Advance Access publication on 8 March 2025
© The Author(s) 2025. Published by Oxford University Press on behalf of Japanese Society of Plant Physiologists.
This is an Open Access article distributed under the terms of the Creative Commons Attribution-NonCommercial License (https://creativecommons.org/licenses/by-nc/4.0/), which permits non-commercial re-use, distribution, and reproduction in any medium, provided the original work is properly cited. For commercial re-use, please contact reprints@oup.com for reprints and translation rights for reprints. All other permissions can be obtained through our RightsLink service via the Permissions link on the article page on our site—for further information please contact journals.permissions@oup.com.

lines, and venation guides) on highly elaborate floral structures such as insectiform labellum of some orchids (Vignolini et al. 2012, Wong et al. 2022a). Beyond pigments, PSM also underpin a plethora of volatiles that are estimated to be in tens of thousands of compounds (Pichersky and Lewinsohn 2011, Schilmiller et al. 2012).

In orchids, unusual volatile natural products often underpin the cases of specific pollinator attraction; however, common floral compounds in unusual blends are also a common feature (Wong et al. 2017b, Perkins et al. 2023). Numerous fatty acid derivatives (e.g. alkanes and alkenes, alcohols, aldehydes), isoprenoids (e.g. cyclic/acyclic mono-/sesqui-terpenes), benzenoids (e.g. phenethyl, phenylpropanes), and potentially amino acid derivatives (e.g. nitrogenous and sulfurous compounds) have been reported as relevant for orchid pollinator attraction. However, while the genetic or biochemical basis for their biosynthesis has been predicted for some cases (Wong et al. 2017a, 2019, Guo et al. 2018), it has only been confirmed for a handful of examples (Schlüter et al. 2011, Sedeek et al. 2016, Xu et al. 2017, Huang et al. 2021). Lineage-specific evolution involving molecular mechanisms such as gene duplication (and divergence), spatiotemporal changes of gene expression, alteration of enzyme activities or subcellular compartmentalization (Ono and Murata 2023) among other mechanisms, likely underpin the ability of orchids to evolve novel and/or fine-tune existing PSM pathways (Schlüter and Schiestl 2008, Schiestl and Schlüter 2009).

The Australian orchid genus *Caladenia* (>350 species) is the only known predominately sexually deceptive (SD) genus to also contain food deceptive (FD) and food rewarding species (Phillips et al. 2009, Weston et al. 2014). Furthermore, there are two recent, parallel radiations containing both FD and SD species within the largest subgenus, *Calonema* (200+ spp.), and the smaller subgenus, *Phlebochilus* (70+ spp.) (Peakall et al. 2021, O'Donnell et al. 2024). Consequently, species exhibit dramatic floral morphology, colour, and volatile/scent (to humans) differences, providing a unique opportunity to explore PSM diversity. In particular, FD *Caladenia* species secure pollination by generalized floral mimicry, often involving several different pollinator species (Phillips et al. 2009). Flowers of FD *Caladenia* species are often strongly scented (to humans) and display brightly coloured (mostly pink, blue/purple, white) hues underpinned by tissue-specific pigmentation chemistry (George et al. 1973, Wong et al. 2024). In contrast, SD *Caladenia* species are dull-coloured (green or maroon) mimics of female insects, have extremely specialized pollinator specificity, often with just a single species of pollinator. Such extreme specificity is largely achieved by sex pheromone mimicry of the female pollinator (Bohman et al. 2016, Peakall et al. 2020, Peakall 2023).

Multidisciplinary approaches bridging chemical and molecular ecology have revolutionized our understanding of the extraordinary diversity of PSM involved in plant–pollinator interactions (Frachon et al. 2021, Wong et al. 2023). Despite its diversity, the molecular basis of PSM implicated in semiochemical and pigment biosynthesis of *Caladenia* orchids has so far only been successfully explored in the male thynnine wasp-pollinated SD *Caladenia plicata* and bee-pollinated FD *Glossodia major*, respectively (Xu et al. 2017, Wong et al. 2024). For example, in *C. plicata* the biosynthesis of (*S*)-β-citronellol (one of two active pollinator attractant) proceeds from the precursor geranyl diphosphate (GPP) in three steps and involves a monoterpene synthase (CpGES1), an alcohol dehydrogenase (CpADH3), and a double-bond reductase (GpGER1) (Xu et al. 2017).

Here, we focus on *Caladenia denticulata*, an uncommon terrestrial orchid nestled in the subgenus *Phlebochilus. Caladenia denticulata* is thought to employ a generalized food deception strategy with hoverflies, small wasps, and native bees as pollinators (Phillips et al. 2009). As the first step toward a systems-level understanding of the volatile chemical diversity and molecular basis of floral scent in *C. denticulata*, we leveraged multi-tissue transcriptomes and floral headspace volatile profiling to ask the following questions: (i) What biochemical pathways are differentially expressed and enriched in the active glandular trichome-rich sepal tips (Tip) and labellum (Lab) tissues versus non-active floral remains (FR)? (ii) What floral volatiles are emitted and do they mirror the active biochemical pathways of tissue-specific floral transcriptomes? (iii) What are the conditions associated with the evolution of complex floral volatile bouquets of FD orchids? Through subsequent functional characterization, our findings allow us to propose the molecular mechanism underpinning *C. denticulata* floral volatile bouquet and discuss the implications of such findings for the evolution of FD and SD in *Caladenia*.

Results

Assembly of a high-quality, tissue-specific floral transcriptome for *C. denticulata*

RNA sequencing followed by the removal of adapter and low-quality sequences yielded a combined total of over 140 million paired-end (2 × 150 bp) reads across the sequenced FR and two glandular trichome-rich tissues—the labellum (Lab), and tip (Tip) libraries. *De novo* transcriptome assembly, redundancy removal, and evidence-based gene set prediction yielded over 28 000 high-quality gene sets from over 198 000 transcripts. Benchmarking Universal Single-Copy Ortholog (BUSCO) assessments with the Embryophyta lineage database (1614 BUSCOs evaluated) indicated high completeness scores for the full *Trinity* transcriptome assembly (92.2%) as well as the reduced *Evidential* gene sets (>91%) containing predicted primary transcripts or valid alternates (Fig. 1a). Of the 28 703 predicted primary transcripts, 27 103 were sufficiently expressed and thus amenable for further downstream statistical analyses as our 'reference floral transcriptome' (Supplementary data S1 & S2).

Further evaluation of the reference floral transcriptome based on phylogenetically informed orthogroups across orchids and coalescent-based species tree inference revealed topologies consistent with recent orchid phylogenomic analysis that

PCP PLANT & CELL PHYSIOLOGY

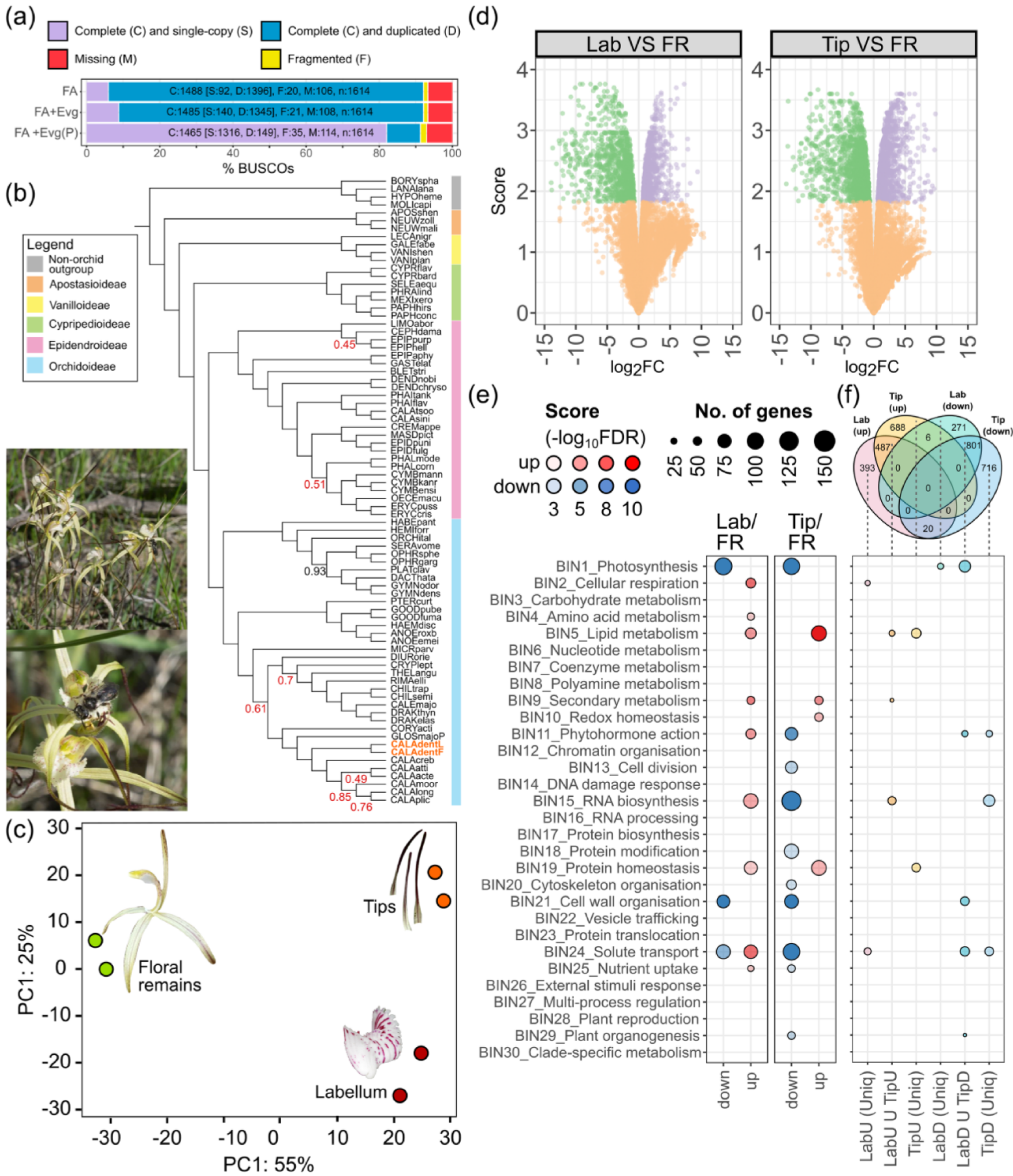

Figure 1. Transcriptomic analysis of *Caladenia denticulata* floral tissues. (a) Gene space completeness of *C. denticulata* floral transcriptomes encompassing floral remains (FR), labellum (Lab), sepal tips (Tip) tissues. BUSCO scores of the full assembly (FA), predicted gene sets of the full assembly (FA + Evg) and final representative primary gene models of the latter [FA + Evg(P)] are shown. (b) The placement of *C. denticulata* on a shortcut coalescent (ASTRAL) species tree of the Orchidaceae (spanning 5 subfamilies, 13 tribes, 21 subtribes and 49 genera) and an outgroup Asparagales taxon. CALAdentL indicate *C. denticulata* assemblies from the leaf (Peakall et al. 2021) while CALAdentF are those obtained from the flowers (this study). Colors indicate orchid subfamily grouping of included genera (see top-left inset). Branch labels indicate local posterior probability (localPP) scores <1. (c) Principal component analysis of the *C. denticulata* floral transcriptome encompassing dissected FR (green), labellum (red), and tip (orange) tissues based on a final set of 27 103 expressed genes. (d) Volcano plot depicting the distribution of differentially expressed genes between putative active labellum (Lab_{VS}FR)—and tip (Tip_{VS}FR) vs non-active FR tissue contrast and associated $\log_2$FC and scores ($-\log_{10}$FDR). Significant upregulation, downregulation (FDR < 0.01), and no differential expression in respective comparisons are indicated by purple, green, and orange colours, respectively. (e) Summary of generalized plant biological processes (Mapman BIN v4 categories) enriched (FDR < 0.01) in significantly up (red) and down (blue)-regulated genes identified in Lab_{VS}FR and Tip_{VS}FR comparisons in (d). Circle size and opacity illustrate the number of annotated genes and enrichment significance of a given enriched category, respectively. (f) Venn diagram summary of unique and common differentially expressed genes in labellum (Lab_{VS}FR)- and tip (Tip_{VS}FR) vs FR tissue contrast and their enriched (FDR < 0.01) Mapman BIN v4 functional categories as in (e).

also span representatives of the subtribe Caladeniinae where *C. denticulata* belongs (Peakall et al. 2021, Wong and Peakall 2022, O'Donnell et al. 2024). They include the pairing of reference floral transcriptome (this study) and previously assembled leaf transcriptome from the same site (Peakall et al. 2021). As expected, *C. denticulata* which belongs to the subgenus *Phlebochilus* was sister to members of subgenus *Calonema* with high confidence (localPP of 1) (Fig. 1b).

Tissue-specific floral transcriptome comparisons and their enriched pathways

Principal component analysis of the *C. denticulata* reference floral transcriptome showed a clear separation of the samples based on tissue type (PC1: 55% and PC2: 25%) with respective samples of FR, Lab, Tip tissues forming distinct groups along both axes (Fig. 1c). Two tissue-specific comparisons/contrasts were prioritized in this study—between non-active FR and active glandular trichome-rich Lab (i. Lab–FR) and Tip (ii. Tip–FR). From the total 27 103 expressed genes, 1509 genes (656 upregulated, 853 downregulated) in Lab–FR contrast and 2126 genes (915 upregulated, 1211 downregulated) in Tip–FR contrasts were differentially expressed (FDR < 0.01) (Fig. 1d, Supplementary data S3). Many PSM-related pathway genes were differentially expressed in the tissue-specific contrasts and contributed to the distinctive signatures of enriched (FDR < 0.05) Mapman BIN v4 categories (Fig. 1e and f, Supplementary data S4).

In the Lab–FR contrast, amino acid metabolism, lipid metabolism, specialized metabolism, and RNA biosynthesis were enriched in upregulated genes. In the Tip–FR contrast, enrichment of lipid metabolism and specialized metabolism were particularly relevant for upregulated genes while phytohormone action and RNA biosynthesis were for downregulated genes. Thus, it is not unexpected that unique and/or down- and upregulated differential expression (DE) gene intersects of such categories are also enriched (Fig. 1f). Nonetheless, biological processes beyond those directly implicated in plant volatile pathways were also enriched in DE genes. These include photosynthesis, redox homeostasis, cellular respiration, cell division, cytoskeleton organization, and cell wall organization (Supplementary data S4).

Spatial dynamics of candidate isoprenoid precursor pathway in the flower

In plants, the plastidial 2-*C*-methyl-D-erythritol 4-phosphate (MEP) pathway and the cytoplasmic-/endoplasmic reticulum-/peroxisomal-localized mevalonate (MVA) pathway are two well-established biosynthetic routes supplying the main building block of all terpenoids, the two 5-carbon building blocks isopentenyl/isoprenyl diphosphate (IPP), and its isomer dimethylallyl diphosphate (DMAPP) (Pichersky and Raguso 2018, Zhou and Pichersky 2020a). Many genes occupying the specialized metabolism terpenoids category (BIN9.1), specifically MVA (BIN9.1.1), MEP (BIN9.1.2), and isoprenyl diphosphate (BIN9.1.3) biosynthesis branch, were DE in both Lab and Tip compared to FR (Fig. 2, Supplementary data S4).

The MVA pathway candidate genes included one acetyl-CoA *C*-acetyltransferase (CdAACT), one 3-hydroxy-3-methylglutaryl-CoA synthase (CdHMGS1), two 3-hydroxy-3-methylglutaryl-CoA reductases (CdHMGR1/2), one MVA kinase (CdMVK), one phospho-MVA kinase (CdPMK), and one diphospho-MVA decarboxylase (CdMPDC). All but *CdMVK* were differentially expressed (Fig. 2, Supplementary data S5 and S6). *CdAACT, CdHMGS1, CdHMGR1*, and *CdPMK* were coordinately upregulated while *CdHMGR2* was downregulated in both Lab and Tip compared to FR, respectively. *CdMPDC* was downregulated and upregulated in the Lab and Tip, respectively, compared to FR. Interestingly, expression of genes encoding the first three steps were among the most highly expressed genes in the Tips (*CdAACT, CdHMGS1, CdHMGR1*), while only *CdHMGR1* was highly expressed in the Lab (Fig. 2).

A total of eight candidate genes encoding MEP pathway enzymes were identified (Fig. 2, Supplementary data S5 and S6). They include two 1-deoxy-D-xylulose 5-phosphate (DXP) synthases (CdDXS1/2), one DXP reductoisomerase (CdDXR), one 2-*C*-methyl-D-erythritol 4-phosphate cytidylyltransferase (CdM CT), one 4-(cytidine 5′-diphospho)-2-*C*-methyl-D-erythritol ki nase (CdCMK), one 2-*C*-methyl-D-erythritol 2,4-cyclodiphosph ate synthase (CdMDS), one 4-hydroxy-3-methylbut-2-enyl-diph osphate (HMBPP) synthase (CmHDS), and one HMBPP reductase (CmHDR). Of the eight, only *CdCMK* was downregulated in the Lab while *CdDXS1, CdCMK*, and *CdHDS* were upregulated in Tip compared to FR. Nonetheless, *CdHDR* was among the most highly expressed genes in both Lab and Tips.

IPP and DMAPP produced from the MVA and MEP pathways are enzymatically interconvertible. The maintenance of this equilibrium is generally performed by IPP isomerase (IDI) which is known to be localized to multiple subcellular compartments (e.g. mitochondria, peroxisome, and plastid). However, emerging studies point towards the involvement of IP kinase in the generation of IPP and DMAPP from IP and DMAP, respectively, in the cytosol, while specific NUDIX hydrolase (NUDX) catalyses the dephosphorylation of IPP and DMAPP (Zhou and Pichersky 2020a). In this study, three IDIs (CdIDI1/2/3), one IPK (CdIPK), and two NUDX (CdNUDX1/3) homologs were found—all of which are predicted to be localized to the cytoplasm except for CdIDI2/3 (plastids) (Supplementary data S6). Interestingly, only *CdIDI2* was specifically upregulated in the Tip compared to FR and was also among the top highly expressed genes in this contrast (Fig. 2).

In plants, the biosynthesis of geranyl diphosphate (GPP) typically occurs in the plastid, farnesyl diphosphate (FPP) in the cytosol, and geranylgeranyl diphosphate (GGPP) across multiple subcellular compartments. Furthermore, short-chain prenyl-PP synthases encoded by gene families (e.g. *GPPS, FPPS, GGPPS*) are typically involved in the addition of IPP(s) to the primary substrate, DMAPP. Here, three plastidial-predicted

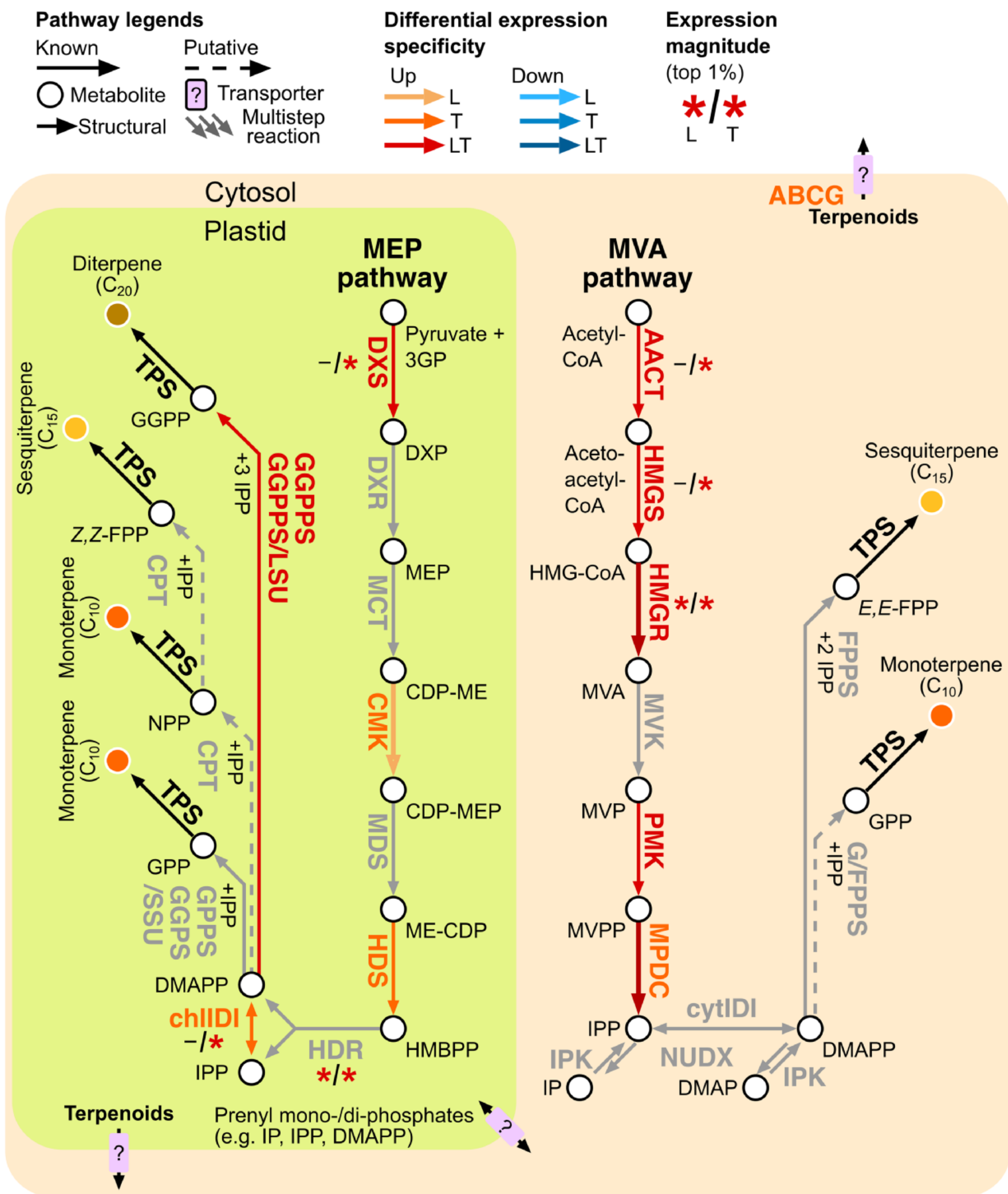

Figure 2. Schematic of putative terpene precursor biosynthesis pathways in *C. denticulata*. Enzymes (bold letters), precursors/products (circles) of the plastid-localized (yellow-green background) methylerythritol phosphate (MEP) and the cytosolic-localized (beige background) mevalonate (MVA) pathway, the two routes for supplying the two 5-carbon building blocks IPP and its isomer DMAPP for various terpenoid-related (e.g. C_5, C_{10}, C_{15}, C_{20}, C_{25}, C_{40}, etc.) compound biosynthesis in plants are indicated. Significant upregulation (light-to-dark blue) and downregulation (light-to-dark red) in the Lab (L), Tip (T), or both (LT) are indicated by different coloured arrows. Grey arrows indicate no differential expression. Asterisk denotes whether their respective gene expression (expressed as FPKM) are within the top 1% of genes with the highest expression (i.e. very highly expressed) in respective labellum (left)/tip (right) tissue transcriptome. Abbreviations—MVA pathway: AACT, acetyl-CoA C-acetyltransferase; HMGS, 3-hydroxy-3-methylglutaryl-CoA synthase; HMGR, 3-hydroxy-3-methylglutaryl-CoA reductase; MVK, MVA kinase; PMK, phospho-MVA kinase; MPDC, diphospho-MVA decarboxylase. MEP pathway: DXS, 1-deoxy-D-xylulose 5-phosphate (DXP) synthase; DXR, DXP reductoisomerase; MCT, 2-C-methyl-D-erythritol 4-phosphate cytidylyltransferase; CMK, 4-(cytidine 5′-diphospho)-2-C-methyl-D-erythritol kinase; MDS, 2-C-methyl-D-erythritol 2,4-cyclodiphosphate synthase; HDS, 4-hydroxy-3-methylbut-2-enyl-diphosphate (HMBPP) synthase; HDR, HMBPP reductase. IPP and DMAPP: IPK, isopentenyl phosphate kinase; NUDX, NUDIX hydrolase; cytIDI, cytoplasmic-localized isopentenyl diphosphate isomerase; chlIDI, chloroplastic-localized IDI; G/FPPS, geranyl/farnesyl diphosphate synthase; GPPS, geranyl diphosphate synthase; GGPPS, geranylgeranyl diphosphate synthase. SSU I, type I small subunit of GPPS; SSU II, type II small subunit of GGPPS; CPT, cis-prenyltransferase. Others: ABCG, adenosine 5′-triphosphate-binding cassette transporter (subfamily G).

candidate genes encoding the *Arabidopsis* homolog of the large (CdGGPPSa/b/c_LSU) and one small (CdGGPPS_SSU) subunit of the heterodimeric GGPP synthase were identified in *C. denticulata*, respectively. One potential bifunctional GPP/FPP synthase (Conart et al. 2023) homolog predicted to localize in the cytosol (CdG/FPPS) was also identified. However, only CdGGPPSb_LSU was coordinately upregulated in the Lab and Tip tissues compared to FR (Fig. 2, Supplementary data S6).

Spatial dynamics of candidate *TPS* gene expression in the flower

Plant TPS are broadly classified into at least eight subfamilies (TPS-a to TPS-h) based on lineage distribution, sequence homology, and function, among others (Chen et al. 2011, Zhou and Pichersky 2020a, Bergman and Dudareva 2024). Phylogenetic analysis of candidate CdTPSs alongside functionally characterized plant TPS across a wide range of angiosperms in various well-established groups indicate that (i) CdTPS-c1, belongs to the TPS-c clade, (ii) CdTPS-e/f1, belongs to the TPS-e/f clade, (iiii) CdTPS-a1/a2, belong to the TPS-a clade, and (iv) CdTPS-b1/b2/b3/b4, belong to the TPS-b clade (Fig. 3a, Supplementary data S7). Expression analysis of the eight candidate *TPS* genes revealed that *CdTPS-c1*, *CdTPS-b1*, and *CdTPS-b2* were lowly expressed regardless of tissue type while *CdTPS-b3* and *CdTPS-b4* were among the most highly expressed genes in both Lab and Tip. *CdTPS-b4* was upregulated in the Tip, while *CdTPS-b3* was upregulated in both Lab and Tip tissues compared to FR (Fig. 3b). As such, CdTPS-b3 and CdTPS-b4 serve as prime candidates for terpene production in *C. denticulata* flowers.

Functional characterization of *C. denticulata* CdTPS-b3 and CdTPS-b4 *in vitro*

The proteins encoded by *CdTPS-b3* and *CdTPS-b4* (without the predicted transit peptide) were produced in *E. coli* and TPS functions were tested *in vitro* using GPP, NPP, *E,E*-FPP, *Z,Z*-FPP, or GGPP as substrates (Fig. 4). Functional assays revealed that CdTPS-b3 mainly catalysed the formation of α-pinene (peak 1) from GPP or NPP and had no activity with *E,E*-FPP, *Z,Z*-FPP, or GGPP. Nonetheless, CdTPS-b3 could also catalyse GPP and/or NPP into a series of minor monoterpene constituents composed of β-pinene (peak 2), β-myrcene (peak 3), D-limonene (peak 4), *trans*-β-ocimene (peak 5), *cis*-β-ocimene (peak 6), linalool (peak 7), α-terpineol (peak 8), geraniol (peak 9), and nerol (peak 10) (Fig. 4, Supplementary data S8).

In contrast, CdTPS-b4 showed activity on all tested substrates including GGPP (Fig. 4). For example, major products formed using GPP include β-myrcene (peak 3), *cis*-β-ocimene (peak 6), and geraniol (peak 9) while NPP produces β-myrcene (peak 3), α-terpineol (peak 8), and nerol (peak 10), among others. α-Farnesene (peak 11) was the only major product produced when supplied with *E,E*,-FPP while diverse sesquiterpenes putatively matching zingiberene (peak 12), α-bergamotene (peak 13), (*E*)-β-farnesene (peak 14), β-sesquiphellandrene (peak 15), β-himachalene (peak 16), β-curcumene (peak 17), 1,4,7,-cycloundecatriene (peak 20) were produced with *Z,Z*-FPP. An unknown diterpene was also produced with the addition of GGPP *in vitro*. Thus, CdTPS-b4 bears hallmarks of a promiscuous TPS (Fig. 4, Supplementary data S8).

Subcellular localization of *C. denticulata* CdTPS-b3 and CdTPS-b4 proteins

To determine the subcellular localizations of CdTPS-b3 and CdTPS-b4, respective N-terminus encompassing the first 100 codons were fused to the N-terminus of eYFP and transiently expressed in *Nicotiana benthamiana* leaves (Fig. 5). Dual localizations of CdTPS-b3 and CdTPS-b4 were observed in both plastid and cytosol albeit a weaker cytosolic signal was often seen for CdTPS-b3. Transient expression of CdTPS-b3-GFP and CdTPS-b4-GFP in *Arabidopsis thaliana* protoplasts consistently exhibit dual localization in both plastid and cytosol (Supplementary Fig. S9). However, it is noteworthy that localization of CdTPS-b4 in the cytosol often appears speckled.

Floral volatile profiles of *C. denticulata* in the natural environment

Caladenia denticulata floral headspace collections were obtained (Fig. 6) and putative terpenoid volatile organic compounds (VOCs) were tentatively identified by comparing the mass spectra obtained from gas chromatography-mass spectrometry (GC-MS) against several reference spectra databases (e.g. NIST-17) and standards where possible. The monoterpene, α-pinene was the dominant headspace floral VOC ($48.1 \pm 3.17\%$), however, a series of mono- and sesquiterpenes were also present in very low ($\sim$1–2%; i.e. α-pinene oxide, terpinen-4-ol, 4-thujanol) or trace quantities (<0.1%; i.e. sabinene, β-pinene, β-myrcene, limonene, verbenone, aromadendrene, α-bergamotene, α-farnesene). Together, the relative abundance of terpenoid-associated VOCs was $\sim$54%. These findings coincide with not only the tissue-specific differential upregulation and enrichment of plant specialized metabolism pathways involving terpenoids (Figs. 2 and 3) but also the potential spectrum of mono- and sesquiterpene compounds catalysed by CdTPS-b3 and CdTPS-b4 (Fig. 4). However, it is noteworthy that other classes of VOCs, especially phenylpropanoid/benzenoids (ca. 22%) and fatty acid derivatives (ca. 20%) were also part of the floral bouquet of *C. denticulata*.

Comparative analysis of functionally characterized CdTPS-b3 and CdTPS-b4 and their homologs in *C. plicata*

Presently, the only other multi-tissue floral transcriptomes in *Caladenia* is for *C. plicata*, a SD species that belong in the largest subgenus *Calonema* (Xu et al. 2017). Mining its transcriptomes revealed a candidate TPS, *C. plicata* TPS-b3 (CpTPS-b3) sharing 96.3% amino acid similarity with CdTPS-b3 (Supplementary

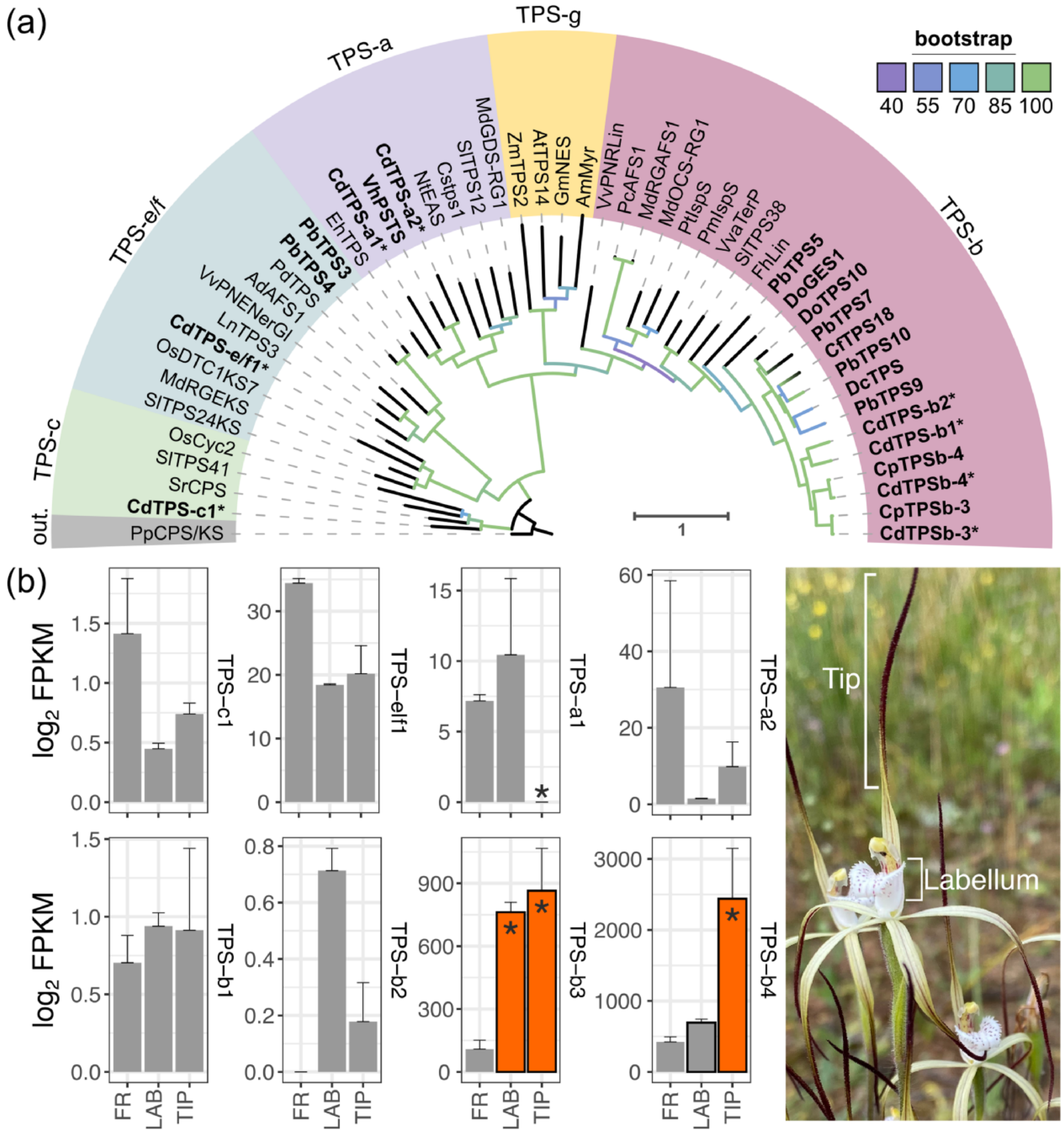

Figure 3. *Caladenia denticulata* TPS gene family. (a) A maximum-likelihood IQTREE phylogeny of putative floral-expressed *C. denticulata* TPS and functionally characterized plant TPS (including other orchids). Colour shading indicate TPS-c (green), TPS-e/f (blue), yellow (TPS-g), purple (TPS-a), salmon pink (TPS-b) clades, respectively and grey indicating an outgroup (out.). Asterisks denote *C. denticulata* putative TPS. Scale bar indicates amino acid substitutions per site. See Supplementary data S7 for associated accession and publication details. (b) Gene expression of putative floral-expressed *C. denticulata* TPS in the floral remains (FR), labellum (Lab), and tip (Tip) tissue. Gene expression in each tissue is expressed as FPKM. Orange bars with asterisks indicate significant upregulation in the labellum and/or tip compared to FR tissues. Borders indicate the top 1% ranked of genes with the highest expression in respective tissue transcriptome (i.e. very highly expressed).

data S10). CpTPS-b3 mainly catalysed the formation of α-pinene from GPP and NPP and had no activity with *E,E*-FPP, *Z,Z*-FPP, or GGPP (Fig. 4). Transient expression of *CpTPS-b3* in *N. benthamiana* leaves also revealed dual localization in both plastid and cytosol (Supplementary data S11). Furthermore, we found that the closest *C. plicata* homolog of CdTPS-b4 that encodes the functionally characterized geraniol synthase (CpGES1) (Xu et al. 2017), sharing 95.2% amino acid similarity with CdTPS-b4 (Supplementary data S10) could also catalyse the formation of additional monoterpenes such as β-myrcene (peak 3), D-limonene (peak 4), α-terpineol (peak 8), nerol (peak 10) using NPP and putative sesquiterpenes α-bergamotene (peak 18), limonen-6-ol, pivalate (peak 19), and 1,4,7,-cycloundecatriene (peak 20) using *Z,Z*-FPP. No activity with *E,E*-FPP, or GGPP was observed for CpGES1/CpTPS-b4 (Fig. 4). Unlike CdTPS-b4, transient expression of *CpGES1/CpTPS-b4* in *N. benthamiana* leaves exhibited exclusive plastid localization (Supplementary data S11). Interestingly, *CpTPS-b4/CpGES1* was the most highly

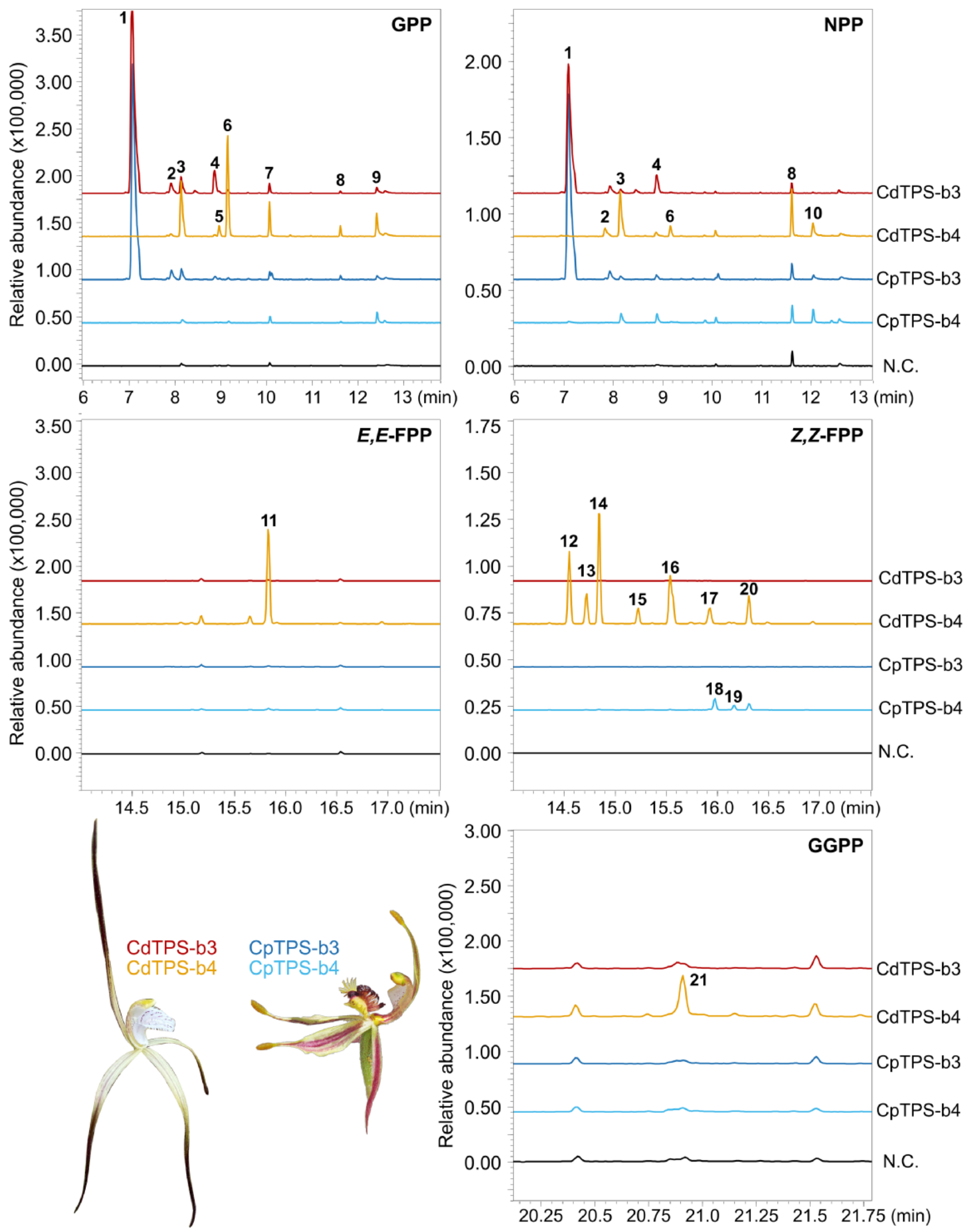

Figure 4. GC–MS analysis of the products formed *in vitro* by the enzymatic activities of *Caladenia* TPS proteins (CdTPS-b3, CdTPS-b4, CpTPS-b3, and CpTPS-b4/CpGES1). Enzymes were incubated with GPP, NPP, *E,E*-FPP, *Z,Z*-FPP, and GGPP and products were analysed as described in the 'Materials and Methods' section, $m/z = 93$ was monitored for terpene products. Reaction products were identified by comparing their mass spectra and retention indices to authentic standards and NIST libraries: 1, α-pinene; 2, β-pinene; 3, β-myrcene; 4, D-limonene; 5, trans-β-ocimene; 6, cis-β-ocimene; 7, linalool; 8, α-terpineol; 9, geraniol; 10, nerol; 11, α-farnesene; 12, zingiberene; 13, α-bergamotene; 14, (E)-β-famesene; 15, β-sesquiphellandrene; 16, β-himachalene, 17, β-curcumene; 18, α-bergamotene-like; 19, limonen-6-ol, pivalate-like; 20, 1,4,7,-cycloundecatriene-like, 21, unknown diterpene. Potential nonspecific products include α-terpineol (peak 8). Mass spectra of the terpene products can be found in Supplementary data S8. GPP, geranyl diphosphate; NPP, neryl diphosphate; *E,E*-FPP, trans-farnesyl diphosphate; *Z,Z*-FPP, cis-farnesyl diphosphate; GGPP, geranylgeranyl diphosphate; TPS, terpene synthase; CdTPS-b3, *C. denticulata* TPS-b3; CdTPS-b4, *C. denticulata* TPS-b4; CpTPS-b3, *C. plicata* TPS-b3; CpTPS-b4/CpGES1, *C. plicata* TPS-b4, N.C., negative control.

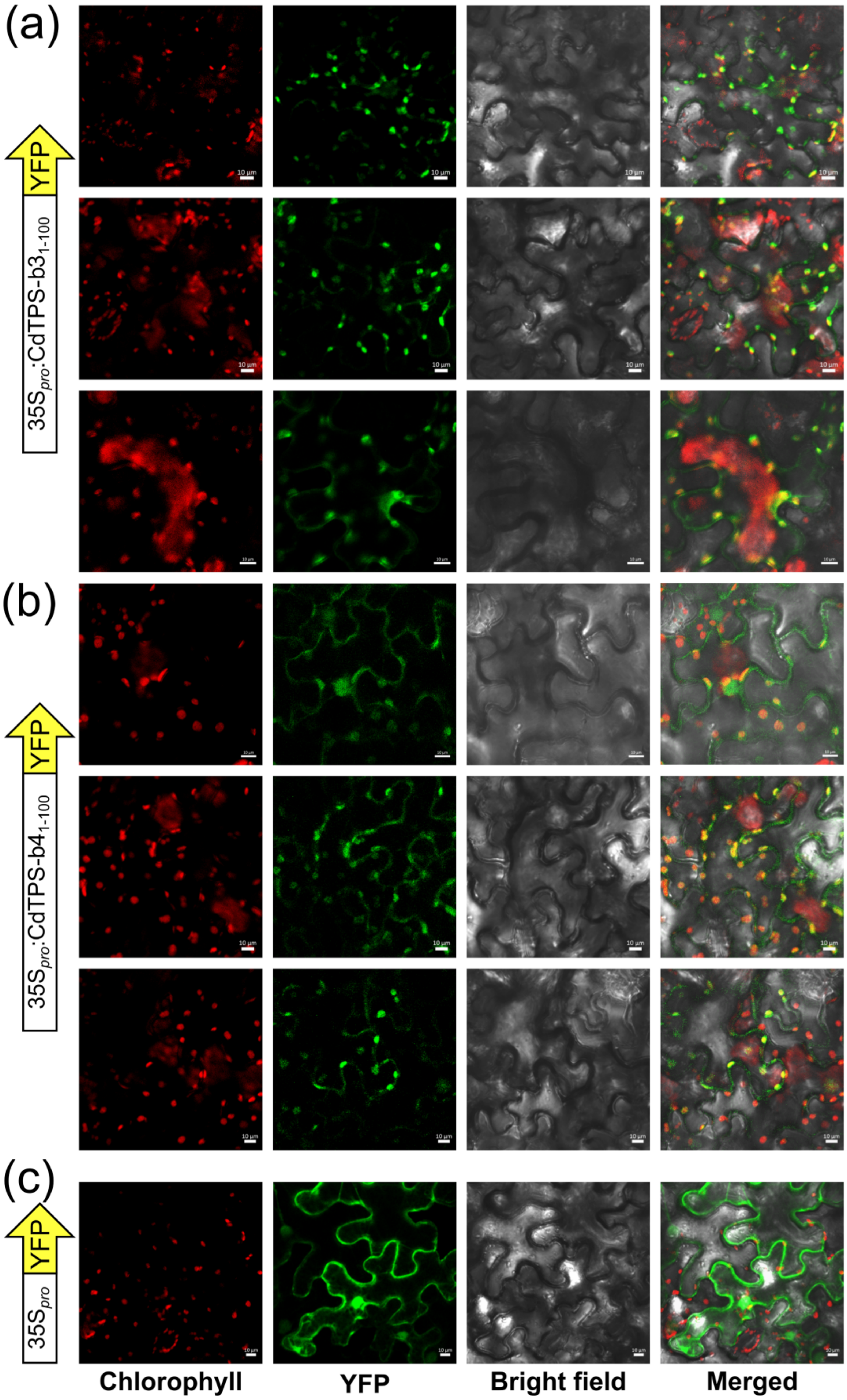

Figure 5. Representative subcellular localization of *C. denticulata* TPS proteins. The first 100 codons of *C. denticulata* (a) TPS-b3 and (b) TPS-b4 were fused to a downstream YFP and transiently expressed in *N. benthamiana* leaves. (C) Unfused YFP construct was used as control. Images were taken by confocal laser scanning microscopy. Each panel (from left to right) depict the autofluorescence from chloroplasts (red), the location of YFP fluorescence of each fusion protein (green), bright field under visible light (grey), and their overlays (merged channels), respectively. A dual localization of CdTPS-b3 and CdTPS-b4 are indicated. Bars, 10 μm.

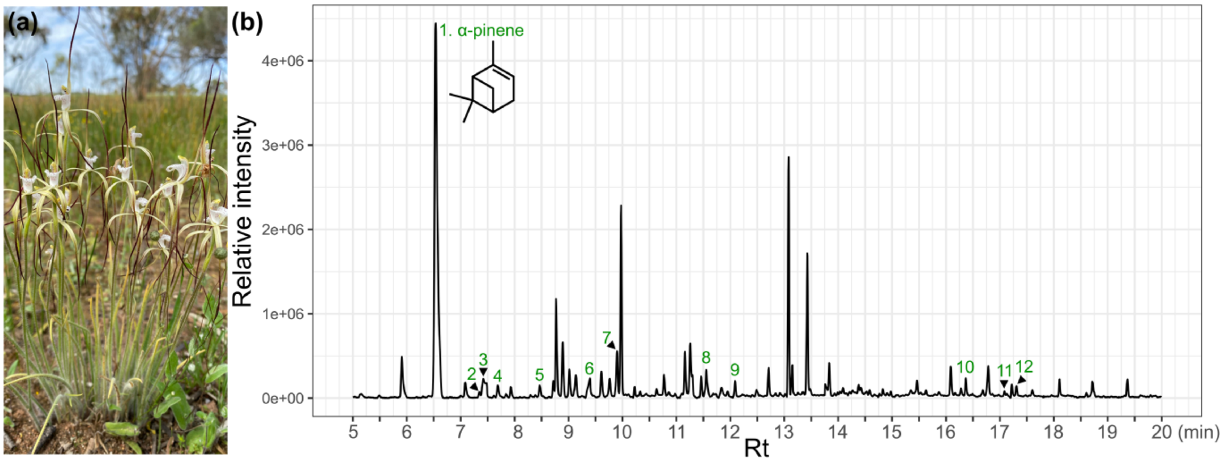

Figure 6. VOCs profile of *C. denticulata* flowers. (a) Representative clump of flowers for headspace collection. (b) Representative total ion chromatograms of *C. denticulata* floral headspace collections extracted in DCM and analysed with GC-MS. Putative terpenoid compounds identified in the headspace samples of *C. denticulata* and associated information on retention time in minutes (Rt_{min}), observed (RI_{obs}), and literature average ($RI_{lit.\ avg.}$) retention index as follows: 1. α-pinene* (6.54, 934, 935), 2. sabinene (7.35, 974, 973), 3. β-pinene (7.41, 978, 978), 4. β-myrcene (7.69, 991, 990), 5. limonene (8.47, 1030, 1030), 6. 4-thujanol (9.3, 1070,1065), 7. α-pinene oxide (9.89, 1100, 1097), 8. terpinen-4-ol* (11.5, 1182, 1179), 9. verbenone (12.1, 1212, 1208), 10. aromadendrene (16.3, 1444, 1438), 11. α-bergamotene (17.1, 1496, n.a.), 12. α-farnesene (17.3, 1509, 1506). * Confirmed with synthetic standards on the same instrument. RI literature values possibly come from a mix of positional isomers.

expressed and upregulated TPS-encoding gene in the swollen glandular sepal tissue that produces citronellol compared to column while *CpTPS-b3* was lowly expressed, up to 30-fold lower than *CpTPS-b4/CpGES1* (Supplementary data S12).

Discussion

The diversity of orchid floral volatiles is staggering with 1000s of compounds spanning diverse biochemical classes (Knudsen et al. 2006). Deciphering the chemical and molecular basis of this diversity is often challenging and best achieved by multidisciplinary collaborations across chemistry, ecology, and genetics (Dötterl and Gershenzon 2023, Perkins et al. 2023, Wong et al. 2023). Chemically mediated orchid floral volatile signals for pollinator attraction often involve numerous compound classes and unique blends, and require finely tuned spatiotemporal regulation of biosynthesis, storage, and/or emission of volatiles (Wong et al. 2017b, Perkins et al. 2023).

New insights into a highly active, tissue-specific terpenoid metabolism pathway of *C. denticulata* flowers

In combination with floral volatile chemical knowledge, new access to several high-quality orchid reference genomes (Zhang et al. 2022) and multi-tissue transcriptomics datasets (ranging in the hundreds to thousands) spanning diverse genera across the orchid family (Wong and Peakall 2022; G. Zhang et al. 2023b) offer unprecedented potential for plant volatile pathway discovery. In particular, floral tissue transcriptome analysis has enabled the initial prioritization, and in some cases confirmation, of diverse volatile-related biochemical pathways involved in the biosynthesis of alkanes and alkenes (Sedeek et al. 2013, 2016), apocarotenoid degradation products (Wang et al. 2022), fatty-acid-derived 2,5-dialkylcyclohexane-1,3-diones (Wong et al. 2017a, 2018, 2019, 2022b), methyl jasmonates (Xu et al. 2019), mono-/sesqui-terpenes (Xu et al. 2017, Chuang et al. 2018a, Huang et al. 2021, Wang et al. 2021), phenylalanine-derived aroma compounds (Gupta et al. 2014, Rao et al. 2014, Yang et al. 2017) as well as volatile emission-related genes (Chang et al. 2023).

In plants, the plastidial MEP are firmly established biosynthetic routes supplying precursor building blocks for the biosynthesis of monoterpene and diterpene while cytoplasmic-/endoplasmic reticulum-/peroxisomal-localized MVA pathways are pivotal for sesquiterpene terpenoids (Pichersky and Raguso 2018, Zhou and Pichersky 2020a). In floral organs, they are often spatiotemporally regulated in a cell-, tissue-, developmental stage-, and rhythmic-specific manner (Livingston et al. 2020, Zhou and Pichersky 2020b, Bechen et al. 2022, Szenteczki et al. 2022, Ling et al. 2023). In this study, we found that most MVA pathway genes were co-ordinately upregulated in both Lab and Tip while MEP pathway genes often showed Tip-specific upregulation compared to FR tissues (Fig. 2). Similar findings characterize the swollen glandular sepal tips of *C. plicata* flowers that accumulate the sex pheromone mimic and pollinator attractant, β-citronellol (a monoterpene alcohol) and 2-hydroxy-6-methylacetophenone (Xu et al. 2017).

Distinct ultrastructural characteristics are often observed at full bloom in terpenoid-rich scent-producing floral tissues of diverse orchids, particularly those with extensive papillae or glandular trichome structures (Hsiao et al. 2006, Arévalo-Rodrigues et al. 2021, Casique et al. 2021, Lipińska et al. 2021, Reposi et al. 2021). These include dense cytoplasmic lipid bodies, plastids rich in starch grains and plastoglobules, an elevated number of mitochondria, and unique endoplasmic reticulum profiles, among others. However, the precise mechanisms by which these ultrastructural properties contribute to specific substrate pools for terpenoid biosynthesis remain unclear in many plant systems (Markus Lange and Turner 2013, Lange 2015, Schuurink and Tissier 2020, Hancock et al. 2024). In our *Caladenia* study species, where we have identified highly active MEP and MVA pathways in the glandular terpenoid-producing floral tissues, future studies still require additional experiments to clarify their carbon supply, particularly towards potential MVA-derived GPP for monoterpene biosynthesis. These may include, but not limited to, histochemical, ultrastructural, MEP/MVA pathway inhibitor, and isotope labelling experiments (Gonçalves-Souza et al. 2017, Maiti and Mitra 2017, Gupta et al. 2024, Zhang et al. 2025). Further multi-omics interrogation of general metabolic pathways (e.g. starch and/or lipid degradation, glycolysis, and the citrate-malate-pyruvate shuttle system) within glandular floral tissues is also warranted (Balcke et al. 2017).

New insights into unique terpene synthases underpinning floral terpenoid volatile biosynthesis of *C. denticulata*

The capacity of TPS enzymes to catalyse single-to-multi-product reactions from a single substrate, their common presence as medium-to-large gene families in genomes (sometimes more than 100 encoded genes), and their spatiotemporal regulation in specific cells, tissues, organs, and/or development stages are well-established factors influencing the generation of terpenoid chemodiversity in plants (Pichersky and Raguso 2018, Zhou and Pichersky 2020a, Bergman and Dudareva 2024). Presently, between 6 and 60 candidate *TPS* genes have been predicted in fewer than a handful of sequenced orchid genomes (Cai et al. 2015, Zhang et al. 2017, Yang et al. 2021) and transcriptomes (Xu et al. 2017, Huang et al. 2021, Wang et al. 2021), indicating there will also be much *TPS* gene diversity across the orchids. In this study, eight candidate genes spanning subfamilies TPS-a/-b/-c/-e/-f/ and -g (Chen et al. 2011) were identified, two of which were very highly expressed in the Lab and Tip (*CdTPS-b3/-b4*), and only *CdTPS-b3* was strongly induced in both tissues compared to the FR (Fig. 3).

In vitro biochemical assays confirmed that CdTPS-b3 and CdTPS-b4 were functional, generating diverse monoterpene and sesquiterpene compounds with a variety of substrates tested (Fig. 4). Notably, *CdTPS-b3* encodes a monoterpene synthase, producing α-pinene from GPP and NPP while CdTPS-b4 alone was capable of catalysing the formation of various monoterpenes (approximately 10 with GPP/NPP), sesquiterpenes (approximately 10 with *E,E,*-FPP/*Z,Z,*-FPP), and an unknown diterpene (with GGPP) *in vitro*. Our findings with CdTPS-b3 and CdTPS-b4 further support the growing evidence that plant TPS enzymes may readily accept *cis*-prenyl substrates (e.g. NPP and *Z,Z*-FPP), challenging the historical view that *trans*-prenyl diphosphates (e.g. GPP and *E,E,*-FPP) were their sole physiological substrates (Zhou and Pichersky 2020a, Bergman and Dudareva 2024).

While most members of the angiosperm-specific TPS-b subfamily often catalyze a single monoterpene product, emerging studies show that some catalyse multi-product reactions from a single substrate and even possess multi-substrate promiscuity (Johnson et al. 2019, Bao et al. 2020, 2023, Li et al. 2021). CdTPS-b4 possesses such properties that are indicative of a *bona fide* promiscuous TPS—a first example of its kind for the Orchidaceae also. In other plant families, floral-expressed *LoTPS4* and *LoTPS7* from *Lathyrus odoratus* (Fabaceae) encode enzymes producing multiple monoterpenes (5 and 11) and sesquiterpenes (6 and 13) from the standard precursors GPP and *E,E*-FPP, respectively. Unexpectedly, they also showed similar activity with the related *cis*-prenyl diphosphates NPP and Z,Z-FPP (Bao et al. 2020).

Beyond enzyme activities, CdTPS-b3 and CdTPS-b4 were further experimentally determined to be dual-localized to the plastid and cytosol (Fig. 5). While such a finding is not unprecedented, it nonetheless raises the possibility of cytosolic monoterpene biosynthesis in plants that defies conventional subcellular compartmentalization (Sun et al. 2016). Indeed, such discoveries appeared more prevalent for short-chain terpene biosynthesis (Zhou and Pichersky 2020a). To date, cytosolic-localized α-pinene synthases are known in strawberries (Aharoni et al. 2004), *Freesia* species (Bao et al. 2023), and roses (Li et al. 2024, Shang et al. 2024) and in most cases, their expression underpins species/cultivar-specific fruit and floral α-pinene accumulation. Other examples of cytosolic-localized mono-/sesqui-TPS include i. the biosynthesis of the monoterpene linalool (FaNES1) in strawberry receptacle tissues (Aharoni et al. 2004), geraniol (LdGES) in *Lippia dulcis* leaves and flowers (Dong et al. 2013), β-ocimene (SlTPS25) in tomato flowers (Zhou and Pichersky 2020b), among others. Further supporting such an unconventional route (vs. MEP-derived GPP) in floral organs is the recent discovery of a potentially widespread MVA-derived GPP precursor supply pathway involving cytosolic bifunctional geranyl/farnesyl diphosphate synthase (G/FPPS) activities in roses (Conart et al. 2023, Li et al. 2024). Alternatively, inter-compartmental transport mechanisms of various terpene precursors (e.g. prenyl mono-/di-phosphates—IP, IPP, DMAPP) that are yet to be established but long predicted (Zhou and Pichersky 2020a), may also be pivotal for α-pinene biosynthesis in *C. denticulata* flowers. Taken together, it is likely that both plastidial and cytosolic route are essential for CdTPS-b3-catalyzed α-pinene biosynthesis—the major floral volatile emitted by *C. denticulata* flowers (Fig. 6).

Although CdTPS-b4 exhibits promiscuous catalytic activity and dual localization in plastids and the cytosol (Figs. 4 and 5), the lack of diverse CdTPS-b4-catalysed terpenoid products (present only in trace amounts or absent altogether) in *C. denticulata* floral headspace suggests a scarcity of available prenyl diphosphate substrates in the floral tissues. Indeed, CcTPS1 from the Himalayan mint shrub (*Colquhounia coccinea*, Lamiaceae) possessed one of the most promiscuous plant TPS known to date and is capable of accepting GPP, FPP, GGPP, and GFPP to form a diverse array of corresponding mono-/sesqui-/di-/sester- terpenoids *in vitro*, respectively (Li et al. 2021). However, as often with promiscuous TPS enzymes (Bergman and Dudareva 2024), only select products (i.e. sesquiterpenes and diterpenes) are present in *Colquhounia coccinea* leaf and floral extracts. While subcellular localization and *in vitro* TPS functional characterization were conducted in routine heterologous model systems, these findings require *in planta* confirmation in *Caladenia* or in other orchid systems. Further studies will also be required to identify candidate short-chain prenyl-diphosphate synthases and confirm which are functional, especially for the supply of *trans* vs *cis*-prenyl diphosphates, and to which subcellular compartment they are localized.

Putative roles of *C. denticulata* terpenoid floral volatiles to potential pollinators

The role of olfactory signals involved in generalized food deception can vary dramatically between orchid species and is by far more challenging to reliably elucidate due to the diversity of VOCs underlying the floral bouquet and potential pollinator(s) involved (Perkins et al. 2023). Attraction in these systems often results from a mixture of compounds, each partially contributing to pollinator attraction. Here, we draw upon the rich chemical ecology literature of plants, but with particular emphasis on orchids, to suggest the potential role of α-pinene that stood out from the complex headspace collections of *C. denticulata*.

The monoterpene, α-pinene has been implicated in several orchid–pollinator interaction (Perkins et al. 2023). For some generalist insect pollinators such as *Bombus terrestris* (bumble bee) that pollinate FD *Orchis mascula* (Dormont et al. 2020), α-pinene was electroantennographic physiologically active (EAD-active). Furthermore, α-pinene (along with β-pinene) is a key floral VOCs emitted by *Epipactis veratrifolia* orchids to mimic aphid alarm pheromones for the attraction of various hoverfly (e.g. *Eupeodes corollae* and *Episyrphus balteatus*) pollinators (Stökl et al. 2011, Jin et al. 2014). Both α- and β-pinene are EAD-active to their *E. balteatus* pollinator (Stökl et al. 2011) and field bioassays using synthetic mixtures of both compounds were attractive to hoverfly pollinators (Jin et al. 2014). Furthermore, field bioassays with the (−)-enantiomer of α-pinene was also attractive to the male euglossine bee *Eulama nigrita*, a key pollinator of scent-rewarding *Stanhopea costaricensis* and *S. ecornuta* orchids (Williams and Whitten 1983).

It is noteworthy that the diverse mixture of low abundance mono- and sesquiterpenes emitted by *C. denticulata* (Fig. 6) are among the most commonly occurring floral volatiles across angiosperms as well as orchids (Knudsen et al. 2006, Schiestl 2010). Although evidence for their role in orchid pollination is limited, these compounds have key roles in pollinator attraction across multiple insect orders (e.g. Coleoptera, Diptera, Hymenoptera, Lepidoptera) and diverse pollination strategies, including both rewarding and deceptive systems (Dötterl and Gershenzon 2023). Interestingly, the floral headspace VOC collections of *C. denticulata* bears strong parallels (i.e. rich in monoterpenes) with those already reported for the FD *C. longicauda* (Salzmann et al. 2006). In the case for *C. longicauda*, these VOCs are likely pivotal for attracting a range of native flies, beetles, bees, and wasps that are frequent visitors and probable pollinators of *C. longicauda* (Phillips et al. 2009, Brundrett 2019). Future studies will require behavioural assays to firmly establish the exact compounds involved in this generalist orchid–pollinator interaction in *Caladenia*.

Potential genetic mechanisms underpinning the evolution of floral volatile bouquets in *Caladenia*

Our findings indicate that in addition to the finely tuned TPS functional promiscuity and subcellular localization plasticity, gene expression differences are another key mechanism underpinning the complex terpenoid VOC production associated with the evolution of deceptive pollination strategies in *Caladenia*. Common floral scent constituents especially terpenoids were either present at very low levels or absent entirely in the flowers of SD species in the subgenus *Calonema* that are known to employ uncommon/novel semiochemicals such as citronellol and 2-hydroxy-6-methylacetophenone in *C. plicata* (Xu et al. 2017) and (methylthio)phenols in *C. crebra* (Bohman et al. 2017) and *C. attingens* (Bohman et al. 2018). In contrast, emission of profiles of FD *C. longicauda* (subgenus *Calonema*) flowers are rich in monoterpenes, especially α/β-pinene derivatives such as α-pinene epoxide, cis-/trans-verbenol, and verbenone (Salzmann et al. 2006).

A comparison of functionally characterized CdTPS-b3/b4 with their *Caladenia plicata* (subgenus *Calonema*) homologs reveals strong conservation of catalytic function and subcellular localization across both subgenera, especially for the TPS-b3 homologs (Figs. 4 and 5). However, regulatory control often differed between the subgenera (Supplementary data S12). Therefore, we predict that strong *Caladenia TPS-b3* homolog expression is one of the few key enabling mechanisms for the gain of terpenoid VOCs observed across both subgenera. In FD *C. denticulata* (subgenus *Phlebochilus*), strong labellum and/or sepal tip-specific *CdTPS-b3* expression appear to be associated with floral volatile profiles rich in pinene-related compounds. A similar involvement of TPS-b3 homologs is envisaged for flowers of FD *C. longicauda*. Conversely, the low expression of *CpTPS-b3* corresponds with the absence of α-pinene derivatives in *C. plicata* flowers, which exhibit high expression of plastid-localized *CpTPS-b4/CpGES1* for the production of geraniol, a key precursor for the accumulation of citronellol (Xu et al. 2017).

The differential expression between *Caladenia* TPS homologs also points to a pivotal role of TFs in the regulation of *TPS* and production of diverse floral terpenoid VOCs. Indeed, diverse transcription factors orchestrate the terpenoid pathway (Chuang et al. 2018b, Dong et al. 2022, Yeh et al. 2022; C. Zhang et al. 2023a) across multiple levels—beginning with precursor supply through to dedicated biosynthesis, decoration/modification, degradation, storage, and even emission. Interestingly, some of these TFs also orchestrate pigment metabolism pathways (Cna'ani et al. 2015, He et al. 2023, Raymond et al. 2018, Shan et al. 2020; C. Zhang et al. 2023a). In the generalized FD orchid genus *Phalaenopsis* (Xiaohua et al. 2012, Pramanik et al. 2020), interspecific variation of floral monoterpene biosynthesis is common and potentially contributes to different bee pollinator attraction (Hsiao et al. 2006). The gain/loss of floral monoterpenes between scented (*P. bellina*) compared to unscented or weakly scented (e.g. *P. equestris*, *P. aphrodite*, and *P. javanica*) species is largely influenced by the regulation of *TPS5* and *TPS10* (geraniol and linalool synthase) (Huang et al. 2021) and precursor biosynthetic pathways by diverse TFs especially *bHLH4* (Chuang et al. 2018b).

Conclusion

In summary, we combined transcriptomic analysis between glandular trichome-rich sepal tips and labellum and non-active flower tissues, phylogenetic analysis of the terpene synthase (TPS) gene family, protein functional assays, and volatile headspace profiling. This comprehensive approach allowed us to investigate the chemical and genetic basis of the strongly scented floral bouquet of pale white/yellow-flowered *C. denticulata* for the very first time. Our findings include: (i) the metabolic pathway specialization for the biosynthesis of commonly occurring floral terpenoids in headspace collections, and (ii) the discovery of dual-localized (plastid and cytosol) monoterpene synthase (CdTPS-b3) that underpins α-pinene biosynthesis—the major floral volatile emitted by this species and a *bona fide* promiscuous TPS (CdTPS-b4) that potentially contribute to diverse low-abundant floral mono- and sesquiterpenes. Comparative analysis of *TPS-b3* and *TPS-b4* homologs in *C. denticulata* (subgenus *Phlebochilus*) and *C. plicata* (subgenus *Calonema*), two species with distinct deceptive pollination strategies, further revealed stark differences in gene expression regulation despite strong conservation of catalytic function and subcellular localization, particularly for *TPS-b3* homologs. We predict that the combination of fine-tuned *TPS* gene expression, functional promiscuity, and subcellular localization at multiple pathway branch points, may have been key players in the evolution of diverse pollination strategies in *Caladenia*.

Materials and Methods

Orchid sampling

Caladenia denticulata (commonly known as the Yellow spider orchid) is endemic to Western Australia and grow in a range of habitats from coastal to mostly inland areas with three nominate subspecies/morphs (i.e. *denticulata, albicans, rubella*) with distinctive tissue-specific floral colouration (Jones 2021). Subspecies *denticulata* is the most common and bear pale yellow petals and sepals. Conversely, subspecies *albicans* and *rubella* have white and maroon petal and sepal colours, respectively. All floral morphs share a common white labellum with maroon-coloured radial stripes and somewhat dark maroon or black petal and sepal tips.

Flowers of *C. denticulata* subspecies *denticulata* (yellow morph) from single populations within the Bulbarnet nature Reserve (WA, Australia) were collected for RNA extraction (2014) and floral volatile extraction (2019 and 2021) during its peak flowering season (Sep—Oct) between 10 am and 2 pm on a warm sunny day (> 20°C). For RNA extraction, freshly picked flowers were presented in sunny and warm conditions (8.30–10.30 am) prior to dissection into the labellum, glandular sepal and petal tips, and all other remaining tissues (i.e. column, sepal, and petal remains; hereafter FR), and immediately snap-frozen in liquid nitrogen and stored in −80°C until further use.

RNA extraction, library construction, and RNA sequencing

Molecular methods prior to RNA sequencing were performed as previously described with minor modifications (Xu et al. 2017, Wong et al. 2017a, 2019). In this study, the inactive FR as one component and the putative pollinator-attracting labellum (Lab) and glandular sepal and petal tips (Tip) were the targets for transcriptomic analysis. Briefly, total RNA was extracted from ground tissues (i.e. pooled from five random flowers) using the RNeasy plant mini kit (QIAGEN, Australia) following the manufacturer's protocol. Two biological replicates (as pools) were obtained for each tissue type (6 samples—2 × Lab, 2 × Tip, 2 × FR).

RNA quantitation and quality confirmation were performed on an Agilent 2100 Bioanalyzer (Agilent, USA). Poly(A) mRNA isolation was achieved with the NEBNext Poly(A) mRNA Magnetic Isolation Module and the construction of respective cDNA libraries were enabled with the NEBnext Ultra RNA Library Prep Kit for Illumina (NEB, Australia), both following the manufacturer's guidelines. Paired-end (2 × 150 bp) sequencing on an Illumina HiSeq 2500 platform (Illumina Technologies, USA) was performed at the Biomolecular Resource Facility (BRF), The Australian National University.

Transcriptome assembly, annotation, and evaluation

Bioinformatics methods were performed as previously described with minor modifications (Wong et al. 2022a, 2024). Briefly, raw PE reads were subjected to a range of quality checks such as adaptor removal, sliding-window trimming, as well as length and quality filtering using fastp v0.23.0 (Chen et al. 2018) with default options except the following: -w 16 -W 10 -M 20 -l 100. *De novo* transcriptome assembly was performed using Trinity v2.13.2 with default options (Haas et al. 2013). Evaluation of gene space completeness was completed with BUSCO v5 (Waterhouse et al. 2018) with default settings except the following: -l embryophyta_odb10 (lineage database) and -m transcriptome (assessment mode). Assembly redundancy filtering, protein-coding prediction, prioritization of accurate gene sets to generate a consensus (reference) assembly was performed using EvidentialGene tr2aacds4 pipeline (Don Gilbert 2013) and default settings and retaining only filtered transcripts categorized as 'okay-sets'. Functional annotation of the reference assembly was performed with MapMan4 functional BIN categories using Mercator4 with default settings (Schwacke et al. 2019) and supplemented with the universal protein knowledgebase (UniProtKB) best-blast hits using the ultra-sensitive option of DIAMOND blastx (Buchfink et al. 2014). Phylotranscriptomic evaluation of the reference assembly was performed as previously described (Wong and Peakall 2022) based off the identification of phylogenetic-informed orthogroups species using OrthoFinder (Emms and Kelly 2019), maximum-likelihood gene tree inference using IQ-TREE v2 (Minh et al. 2020), and coalescent-based species tree inference using ASTRAL-III (Yin et al. 2019). Tree visualization was performed with iTOL v4 (Letunic and Bork 2019).

Transcriptome differential expression analysis

Indexing of the reference assembly was performed using bowtie2 (Langmead and Salzberg 2012) followed by end-to-end paired-end read alignment with default options except the following: -end-to-end, -no-mixed, -no-discordant. Read counts summarization was performed using FeatureCounts (Liao et al.

2014) with default options except the following: -B -C -d 100 -P -p—count read pairs. DE analysis between treatments (i.e. Lab–FR and Tip–FR contrasts) following the quasi-likelihood F-test framework was performed in R (http://www.r-project.org) using the edgeR package (Robinson et al. 2009). Up- ($\log_2$FC > 0) and down- ($\log_2$FC < 0) regulated genes satisfying a false discovery rate (FDR) threshold < 1% is deemed differentially expressed in respective contrasts. For visualization, the Fragments Per Kilobase of transcript per Million mapped reads (FPKM) were used as the unit of gene expression. Enriched MapMan4 functional BIN functional categories (FDR < 0.05) in up- and down-regulated genes of respective contrasts were determined based on a hypergeometric distribution adjusted with FDR in R as previously described (Wong et al. 2024).

Isolation of full-length TPS, recombinant protein production, and enzymatic assays

The full-length *C. denticulata* TPS (*CdTPS-b3* and *CdTPS-b4*) open reading frames were amplified from the Lab and Tip cDNA libraries with gene-specific PCR primers (Supplementary data S13) using the Phusion® High-Fidelity DNA Polymerase according to manufacturer's guidelines (NEB, Australia). For *C. plicata, Escherichia coli* codon-optimized versions of *CpTPS-b3* (NCBI GenBank: MF037225) and *CpTPS-b4* were synthesized by GENEWIZ (China). Recombinant protein production and enzymatic assays were performed as previously described with minor modifications (Xu et al. 2017, Zhou and Pichersky 2020b). Briefly, N-terminal truncated TPS cDNAs were cloned into pMAL-c5X plasmid to enable the expression of an N-terminus MBP-tagged TPS recombinant protein. Plasmid constructs were then transformed into *E. coli* Rosetta2(DE3)pLySs cells (Novagen, USA) and grown in LB broth at 37°C. Induction of recombinant proteins was achieved with an overnight incubation using 0.1 mM IPTG at 16°C. Purification of recombinant proteins was achieved using amylose resin (NEB, USA) according to the manufacturer's instruction. TPS enzyme assays were conducted in a reaction mixture containing 20 µg affinity-purified MBP-tagged enzyme, 50 mM HEPES, pH 7.0, 5 mM DTT, 100 mM KCl, and 7.5 mM $MgCl_2$, containing 20 µM of substrates (GPP, NPP, *E,E*-FPP, *Z,Z*-FPP or GGPP) in a final volume of 0.2 ml. Assays were incubated for 60 min at 30°C and reaction products were extracted with methyl tert-butyl ether and analysed on a Shimadzu QP-2020NX GC-MS system (Shimadzu, Japan) fitted with a Rxi-5Sil column (30 m length, 0.25 mm i.d., and 0.25 µm film thickness; Restek). Assays containing purified MBP-tag only (empty vector) recombinant protein were used as negative control.

Phylogenetic analysis

Multiple sequence alignment of predicted *C. denticulata* TPS and a collection of functionally characterized plant TPS proteins (retrieved from NCBI GenBank) was performed using MAFFT v7 (Katoh and Standley 2013) with the L-INS-I option. Maximum-likelihood phylogenetic tree inference was performed with IQ-TREE v2 (Minh et al. 2020) and branch support were obtained with the ultrafast bootstrap approximation (Hoang et al. 2018) based off 1000 iterations. Tree visualization was performed with iTOL v4 (Letunic and Bork 2019).

Subcellular localization

Nicotiana benthamiana and *Arabidopsis* protoplast transformation and confocal microscopy were performed as previously described (Falara et al. 2011, Zhou and Pichersky 2020b). Briefly, the region corresponding to the first 100 codons of CdTPS-b3 and CdTPS-b4 ORFs were amplified with the primer pairs (Supplementary data S13), digested accordingly, and ligated into the pCNHP-eYFP and pA7-YFP vector to create an in-frame C-terminal fusion with eYFP (CdTPS-ORFloc-eYFP). *Agrobacterium tumefaciens* strain GV3101 was transformed and used for infecting *N. benthamiana* mesophyll cells as reported (Zhou and Pichersky 2020b). *Arabidopsis* mesophyll protoplasts were transformed by PEG-mediated method as described before (Zhou and Pichersky 2020b). Three independent transient expression experiments were performed. Fluorescence signals (i.e. 500–530 nm for eYFP and 680–720 nm for chloroplast autofluorescence) were visualized using a Leica SP5 laser scanning confocal microscope as described previously (Falara et al. 2011). Subcellular localization prediction for candidate proteins was performed with TargetP using the Plant (Organism group) option (https://services.healthtech.dtu.dk/services/TargetP-2.0/).

Metabolite analysis & data processing

Floral headspace analysis broadly followed the approach of Salzmann et al. (2006) with modifications. Briefly, sampling was performed on clumps of flowers (min. 12 individuals/clump) in their natural environment at temperature between 20–22°C where floral scent is detectable to the human nose (smelling sweet). PorapakQ volatile traps (117 mg, 5 mm diameter, 30 mm length, SKC inc., Australia) were used with a calibrated a flow rate of 200 mL/min flow rate for 2–5 h. Similarly, control air samples were collected at the same time adjacent to the sampled clumps. Traps were eluted twice with 500 µl DCM, and then again with 1000 µL DCM. Elutions were concentrated to approximately 50 µl prior to analysis. Gas chromatography-mass spectrometry (GC-MS) was used to separate and identify compounds present in headspace of *C. denticulata*. Samples were injected in pulsed splitless mode with inlet held at 250°C into an 8860 Gas Chromatography system connected to a 59 778 Mass Selective Detector (Agilent Australia) equipped with a HP-5 MS UI capillary column (30 m × 0.25 mm × 0.25 µm film thickness; Agilent Australia). Samples were analysed with a constant flow rate of 1.2 ml/min of Helium, with column oven temperature programming as follows: 40°C for 1 min, followed by 7.5°C/min ramp to 325°C, held for 6 min, resulting in a 45 min total run time. The MSD transfer line temperature was 250°C, MS source 230°C, and Quadrupole temp 150°C. Data were collected in scan mode, with a scan range of 50–550 *m/z*. A series of *n*-alkanes from C8 to C44 (Agilent Australia, 10 ng/µl) were used to determine retention indices of detected compounds. MassHunter Qualitative Analysis Software Version 10.0 (Agilent Australia) was used to detect and identify compounds. Compounds were tentatively identified by comparison of mass spectra and retention indicies with data from the NIST17 library, and some compounds were confirmed by direct comparison to synthetic standards. The area counts from integrated TICs were then used to calculate the relative proportions of all detected compounds. Prior to determining relative amounts, area counts of compounds detected in controls were subtracted from the samples. Additionally, the literature average Retention Index (RI) values were calculated by using the *webchem* package (Szöcs et al. 2020) in R to compile all comparable RI values available on the NIST web database (https://www.nist.gov/).

Acknowledgments

We thank Lyn Alcock for photographs of *C. denticulata* with potential native bee pollinators (Fig. 1b) and Ryan D. Phillips for assistance during field sampling.

Author contributions

D.C.J.W., F.Z., E.P., and R.P. designed the study and secured funding. F.Z., J.P., Y.N.Z., H.Y.X., R.P., and D.C.J.W. performed the research. D.C.J.W., J.P., and F.Z. analysed the data. D.C.J.W. wrote the article with assistance from F.Z., E.P., and R.P.

Supplementary data

Supplementary data is available at *PCP* online.

Conflict of interest. None declared.

Funding

This work was supported by the Australian Research Council projects DE190100249 (to D.W.) and DP150102762 and DP210100471 (to R.P. and E.P.), National Natural Science Foundation of China 32300230, and Natural Science Foundation of Jiangsu Province BK20230785 to (F.Z.).

Data Availability

The raw RNA-seq data presented in this study can be found within the NCBI BioProject accession PRJNA1143090 (https://www.ncbi.nlm.nih.gov/bioproject/). Full- length coding sequences of *Caladenia denticulata TPS-b3* (*CdTPS-b3*) and *Caladenia plicata TPS-b3* (*CpTPS-b3*), *C. denticulata CdTPS-b4* have been deposited in NCBI GenBank (https://www.ncbi.nlm.nih.gov/genbank/) under the accessions: PV089060, PV089061, PV089062, respectively.

References

Ackerman, J.D., Phillips, R.D., Tremblay, R.L., Karremans, A., Reiter, N., Peter, C.I., et al. (2023) Beyond the various contrivances by which orchids are pollinated: global patterns in orchid pollination biology. *Bot. J. Linn. Soc.* 202: 295–324.

Aharoni, A., Giri, A.P., Verstappen, F.W.A., Bertea, C.M., Sevenier, R., Sun, Z., et al. (2004) Gain and loss of fruit flavor compounds produced by wild and cultivated strawberry species. *Plant Cell* 16: 3110–3131.

Arévalo-Rodrigues, G., de Barros, F., Davis, A.R. and Cardoso-Gustavson, P. (2021) Floral glands in myophilous and sapromyophilous species of Pleurothallidinae (Epidendroideae, Orchidaceae)—osmophores, nectaries, and a unique sticky gland. *Protoplasma* 258: 1061–1076.

Balcke, G.U., Bennewitz, S., Bergau, N., Athmer, B., Henning, A., Majovsky, P., et al. (2017) Multi-omics of tomato glandular trichomes reveals distinct features of central carbon metabolism supporting high productivity of specialized metabolites. *Plant Cell* 29: 960–983.

Bao, T., Kimani, S., Li, Y., Li, H., Yang, S., Zhang, J., et al. (2023) Allelic variation of terpene synthases drives terpene diversity in the wild species of the *Freesia* genus. *Plant Physiol.* 192: 2419–2435.

Bao, T., Shadrack, K., Yang, S., Xue, X., Li, S., Wang, N., et al. (2020) Functional characterization of terpene synthases accounting for the volatilized-terpene heterogeneity in *Lathyrus odoratus* cultivar flowers. *Plant Cell Physiol.* 61: 1733–1749.

Bechen, L.L., Johnson, M.G., Broadhead, G.T., Levin, R.A., Overson, R.P., Jogesh, T., et al. (2022) Differential gene expression associated with a floral scent polymorphism in the evening primrose *Oenothera harringtonii* (Onagraceae). *BMC Genomics* 23: 1–17.

Bergman, M.E. and Dudareva, N. (2024) Plant specialized metabolism: diversity of terpene synthases and their products. *Curr. Opin.Plant. Biol.* 81: 102607.

Bohman, B., Flematti, G.R., Barrow, R.A., Pichersky, E. and Peakall, R. (2016) Pollination by sexual deception—it takes chemistry to work. *Curr. Opin.Plant. Biol.* 32: 37–46.

Bohman, B., Phillips, R.D., Flematti, G.R., Barrow, R.A. and Peakall, R. (2017) The spider orchid *Caladenia crebra* produces sulfurous pheromone mimics to attract its male wasp pollinator. *Angew. Chem. Int. Educ.* 56: 8455–8458.

Bohman, B., Phillips, R.D., Flematti, G.R. and Peakall, R. (2018) (Methylthio)phenol semiochemicals are exploited by deceptive orchids as sexual attractants for *Caampylothynnus* thynnine wasps. *Fitoterapia* 126: 78–82.

Brundrett, M.C. (2019) A comprehensive study of Orchid seed production relative to pollination traits, plant density and climate in an urban reserve in Western Australia. *Diversity* 11: 123.

Buchfink, B., Xie, C. and Huson, D.H. (2014) Fast and sensitive protein alignment using DIAMOND. *Nat. Methods* 12: 59–60.

Cai, J., Liu, X., Vanneste, K., Proost, S., Tsai, W.-C., Liu, K.-W., et al. (2015) The genome sequence of the orchid *Phalaenopsis equestris*. *Nat. Genet.* 47: 65–72.

Casique, J.V., Andrade, E.H.D.A., De Aguiar Dias, A.C.A. and Mastroberti, A.A. (2021) Novelties in the secretory structures of three species of *Gongora* (Orchidaceae: Stanhopeinae). *Bot. J. Linn. Soc.* 195: 650–670.

Chang, Y.L., Huang, L.M., Kuo, X.Z., Chen, Y.Y., Lin, S.T., Jeng, M.F., et al. (2023) PbABCG1 and PbABCG2 transporters are required for the emission of floral monoterpenes in *Phalaenopsis bellina*. *Plant J.* 114: 279–292.

Chen, F., Tholl, D., Bohlmann, J. and Pichersky, E. (2011) The family of terpene synthases in plants: a mid-size family of genes for specialized metabolism that is highly diversified throughout the kingdom. *Plant J.* 66: 212–229.

Chen, S., Zhou, Y., Chen, Y. and Gu, J. (2018) Fastp: an ultra-fast all-in-one FASTQ preprocessor. *Bioinformatics* 34: i884–i890.

Chuang, Y.C., Hung, Y.C., Hsu, C.Y., Yeh, C.M., Mitsuda, N., Ohme-Takagi, M., et al. (2018a) A dual repeat cis-element determines expression of GERANYL DIPHOSPHATE SYNTHASE for monoterpene production in phalaenopsis orchids. *Front. Plant Sci.* 9: 1–14.

Chuang, Y.C., Hung, Y.C., Tsai, W.C., Chen, W.H. and Chen, H.H. (2018b) PbbHLH4 regulates floral monoterpene biosynthesis in *Phalaenopsis* orchids. *J. Exp. Bot.* 69: 4363–4377.

Cna'ani, A., Spitzer-Rimon, B., Ravid, J., Farhi, M., Masci, T., Aravena-Calvo, J., et al. (2015) Two showy traits, scent emission and pigmentation, are finely coregulated by the MYB transcription factor PH4 in petunia flowers. *New Phytologist* 208: 708–714.

Conart, C., Bomzan, D.P., Huang, X.-Q., Bassard, J.-E., Paramita, S.N., Saint-Marcoux, D., et al. (2023) A cytosolic bifunctional geranyl/farnesyl diphosphate synthase provides MVA-derived GPP for geraniol biosynthesis in rose flowers. *Proc. Natl. Acad. Sci. U. S. A.* 120: e2221440120.

Dong, L., Miettinen, K., Goedbloed, M., Verstappen, F.W.A., Voster, A., Jongsma, M.A., et al. (2013) Characterization of two geraniol synthases from *Valeriana officinalis* and *Lippia dulcis*: similar activity but difference in subcellular localization. *Metab. Eng.* 20: 198–211.

Dong, Y., Zhang, W., Li, J., Wang, D., Bai, H., Li, H., et al. (2022) The transcription factor LaMYC4 from lavender regulates volatile terpenoid biosynthesis. *BMC Plant Biol.* 22: 1–15.

Dormont, L., Fort, T., Bessière, J.M., Proffit, M., Garcia Hidalgo, E., Buatois, B., et al. (2020) Sources of floral scent variation in the food-deceptive orchid *Orchis mascula*. *Acta Oecologica* 107: 103600.

Dormont, L., Joffard, N. and Schatz, B. (2019) Intraspecific variation in floral color and odor in orchids. *Int. J. Plant Sci.* 180: 1036–1058.

Dötterl, S. and Gershenzon, J. (2023) Chemistry, biosynthesis and biology of floral volatiles: roles in pollination and other functions. *Nat. Prod. Rep.* 40: 1901–1937.

Emms, D.M. and Kelly, S. (2019) OrthoFinder: Phylogenetic orthology inference for comparative genomics. *Genome Biol.* 20: 238.

Falara, V., Akhtar, T.A., Nguyen, T.T.H., Spyropoulou, E.A., Bleeker, P.M., Schauvinhold, I., et al. (2011) The tomato terpene synthase gene family. *Plant Physiol.* 157: 770–789.

Frachon, L., Stirling, S.A., Schiestl, F.P. and Dudareva, N. (2021) Combining biotechnology and evolution for understanding the mechanisms of pollinator attraction. *Curr. Opin. Biotechnol.* 70: 213–219.

George, A., Gonzales, C., Strauss, M.S. and Arditti, J. (1973) Chemotaxonomic and ecological implications of anthocyanins in *Elythranthera*. *Biochem. Syst. Ecol.* 1: 45–49.

Gilbert, D. (2013) EvidentialGene: tr2aacds, mRNA transcript assembly software [WWW Document]. http://arthropods.eugenes.org/EvidentialGene/trassembly.html (November 1, 2023, date last accessed).

Gonçalves-Souza, P., Schlindwein, C., Dötterl, S. and Paiva, E.A.S. (2017) Unveiling the osmophores of *Philodendron adamantinum* (Araceae) as a means to understanding interactions with pollinators. *Ann. Bot.* 119: 533–543.

Guo, -Y.-Y., Zhang, Y.-Q., Zhang, G.-Q., Huang, L.-Q. and Liu, Z.-J. (2018) Comparative transcriptomics provides insight into the molecular basis of species diversification of section Trigonopedia (*Cypripedium*) on the Qinghai-Tibetan Plateau. *Sci. Rep.* 8: 11640.

Gupta, A.K., Schauvinhold, I., Pichersky, E. and Schiestl, F.P. (2014) Eugenol synthase genes in floral scent variation in *Gymnadenia* species. *Funct. Integr. Genomics* 14: 779–788.

Gupta, P., Sharma, A., Kiran, N.R., Pranav Raj, T.K., Krishna, R. and Nagegowda, D.A. (2024) Phylogenetically distant enzymes localized in cytosol and plastids drive citral biosynthesis in lemongrass. *Plant J.* 120: 1901–1919.

Haas, B.J., Papanicolaou, A., Yassour, M., Grabherr, M., Blood, P.D., Bowden, J., et al. (2013) De novo transcript sequence reconstruction from RNA-seq using the Trinity platform for reference generation and analysis. *Nat. Protoc.* 8: 1494–1512.

Hancock, J., Livingston, S.J. and Samuels, L. (2024) Building a biofactory: constructing glandular trichomes in *Cannabis sativa*. *Curr. Opin. Plant. Biol.* 80: 102549.

He, G., Zhang, R., Jiang, S., Wang, H. and Ming, F. (2023) The MYB transcription factor RcMYB1 plays a central role in rose anthocyanin biosynthesis. *Hortic. Res.* 10: uhad080.

Hoang, D.T., Chernomor, O., Von Haeseler, A., Minh, B.Q. and Vinh, L.S. (2018) UFBoot2: improving the ultrafast bootstrap approximation. *Mol. Biol. Evol.* 35: 518–522.

Hsiao, -Y.-Y., Tsai, W.-C., Kuoh, C.-S., Huang, T.-H., Wang, H.-C., Wu, T.-S., et al. (2006) Comparison of transcripts in *Phalaenopsis bellina* and *Phalaenopsis equestris* (Orchidaceae) flowers to deduce monoterpene biosynthesis pathway. *BMC Plant Biol.* 6: 14.

Huang, H., Kuo, Y.W., Chuang, Y.C., Yang, Y.P., Huang, L.M., Jeng, M.F., et al. (2021) Terpene synthase-b and terpene synthase-e/f genes produce monoterpenes for *Phalaenopsis bellina* floral scent. *Front. Plant Sci.* 12: 700958.

Jersáková, J., Johnson, S.D. and Kindlmann, P. (2006) Mechanisms and evolution of deceptive pollination in orchids. *Biol. Rev.* 81: 219–235.

Jin, X.-H., Ren, Z.-X., Xu, S.-Z., Wang, H., Li, D.-Z. and Li, Z.-Y. (2014) The evolution of floral deception in *Epipactis veratrifolia* (Orchidaceae): from indirect defense to pollination. *BMC Plant Biol.* 14: 63.

Johnson, S.R., Bhat, W.W., Sadre, R., Miller, G.P., Garcia, A.S. and Hamberger, B. (2019) Promiscuous terpene synthases from *Prunella vulgaris* highlight the importance of substrate and compartment switching in terpene synthase evolution. *New Phytologist* 223: 323–335.

Jones, D.L. (2021) A Complete Guide to Native Orchids of Australia. 3rd edn. New Holland Publishers (South Turramurra, New South Wales, Australia).

Katoh, K. and Standley, D.M. (2013) MAFFT multiple sequence alignment software version 7: improvements in performance and usability. *Mol. Biol. Evol.* 30: 772–780.

Knudsen, J.T., Eriksson, R., Gershenzon, J. and Ståhl, B. (2006) Diversity and distribution of floral scent. *Bot. Rev.* 72: 1–120.

Lange, B.M. (2015) The evolution of plant secretory structures and emergence of terpenoid chemical diversity. *Annu. Rev. Plant Biol.* 66: 139–159.

Langmead, B. and Salzberg, S.L. (2012) Fast gapped-read alignment with Bowtie 2. *Nat. Methods* 9: 357–359.

Letunic, I. and Bork, P. (2019) Interactive Tree of Life (iTOL) v4: recent updates and new developments. *Nucleic Acids Res.* 47: 256–259.

Li, B.J., Zheng, B.Q., Wang, J.Y., Tsai, W.C., Lu, H.C., Zou, L.H., et al. (2020) New insight into the molecular mechanism of colour differentiation among floral segments in orchids. *Commun. Biol.* 3: 1–13.

Li, D.S., Hua, J., Luo, S.H., Liu, Y.C., Chen, Y.G., Ling, Y., et al. (2021) An extremely promiscuous terpenoid synthase from the Lamiaceae plant *Colquhounia coccinea* var. mollis catalyzes the formation of sester-/di-/sesqui-/mono-terpenoids. *Plant Commun.* 2: 100233.

Li, H., Li, Y., Yan, H., Bao, T., Shan, X., Caissard, J.-C., et al. (2024) The complexity of volatile terpene biosynthesis in roses: Particular insights into β-citronellol production. *Plant Physiol.* 196: 1908–1922.

Liang, C.Y., Rengasamy, K.P., Huang, L.M., Hsu, C.C., Jeng, M.F., Chen, W.H., et al. (2020) Assessment of violet-blue color formation in *Phalaenopsis* orchids. *BMC Plant Biol.* 20: 1–16.

Liao, Y., Smyth, G.K. and Shi, W. (2014) FeatureCounts: an efficient general purpose program for assigning sequence reads to genomic features. *Bioinformatics* 30: 923–930.

Ling, Z., Li, J., Dong, Y., Zhang, W., Bai, H., Li, S., et al. (2023) Terpene produced by coexpression of the TPS and P450 genes from *Lavandula angustifolia* protects plants from herbivore attacks during budding stages. *BMC Plant Biol.* 23: 1–13.

Lipińska, M.M., Wiśniewska, N., Gołębiowski, M., Narajczyk, M. and Kowalkowska, A.K. (2021) Floral micromorphology, histochemistry, ultrastructure and chemical composition of floral secretions in three Neotropical *Maxillariella* species (Orchidaceae). *Bot. J. Linn. Soc.* 196: 53–80.

Liu, Y.C., Yeh, C.W., Chung, J.D., Tsai, C.Y., Chiou, C.Y. and Yeh, K.W. (2019) Petal-specific RNAi-mediated silencing of the phytoene synthase gene reduces xanthophyll levels to generate new *Oncidium* orchid varieties with white-colour blooms. *Plant Biotechnol. J.* 17: 2035–2037.

Livingston, S.J., Quilichini, T.D., Booth, J.K., Wong, D.C.J., Rensing, K.H., Laflamme-Yonkman, J., et al. (2020) Cannabis glandular trichomes alter morphology and metabolite content during flower maturation. *Plant J.* 101: 37–56.

Maiti, S. and Mitra, A. (2017) Morphological, physiological and ultrastructural changes in flowers explain the spatio-temporal emission of scent volatiles in *Polianthes tuberosa* L. *Plant Cell Physiol.* 58: 2095–2111.

Markus Lange, B. and Turner, G.W. (2013) Terpenoid biosynthesis in trichomes-current status and future opportunities. *Plant Biotechnol. J.* 11: 2–22.

Minh, B.Q., Schmidt, H.A., Chernomor, O., Schrempf, D., Woodhams, M.D., Von Haeseler, A., et al. (2020) IQ-TREE 2: new models and efficient methods for phylogenetic inference in the genomic era. *Mol. Biol. Evol.* 37: 1530–1534.

O'Donnell, R.P., Wong, D.C.J., Phillips, R.D., Peakall, R., Linde, C.C. (2024) Discordance down under: combining phylogenomics & fungal symbioses to detangle difficult nodes in a diverse tribe of Australian terrestrial orchids. *Syst. Biol.* 73: 1–20.

Ono, E. and Murata, J. (2023) Exploring the evolvability of plant specialized metabolism: uniqueness out of uniformity and uniqueness behind uniformity. *Plant Cell Physiol.* 64: 1449–1465.

Peakall, R. (2023) Pollination by sexual deception. *Curr. Biol.* 33: R489–R496.

Peakall, R., Wong, D.C.J., Bohman, B., Flematti, G.R. and Pichersky, E. (2020) Floral volatiles for pollinator attraction and speciation in sexually deceptive orchids. *In* Biology of Plant Volatiles Edited by Pichersky, E. and Dudareva, N. pp. 271–295. CRC Press (Boca Raton, Florida, U.S.A).

Peakall, R., Wong, D.C.J., Phillips, R.D., Ruibal, M., Eyles, R., Rodriguez-Delgado, C., et al. (2021) A multitiered sequence capture strategy spanning broad evolutionary scales: Application for phylogenetic and phylogeographic studies of orchids. *Mol. Ecol. Resour.* 21: 1118–1140.

Perkins, J., Hayashi, T., Peakall, R., Flematti, G.R. and Bohman, B. (2023) The volatile chemistry of orchid pollination. *Nat. Prod. Rep*. 40: 819–839.

Phillips, R.D., Faast, R., Bower, C.C., Brown, G.R. and Peakall, R. (2009) Implications of pollination by food and sexual deception for pollinator specificity, fruit set, population genetics and conservation of *Caladenia* (Orchidaceae). *Aust. J. Bot*. 57: 287–306.

Pichersky, E. and Lewinsohn, E. (2011) Convergent evolution in plant specialized metabolism. *Annu. Rev. Plant Biol*. 62: 549–566.

Pichersky, E. and Raguso, R.A. (2018) Why do plants produce so many terpenoid compounds?. *New Phytologist* 220: 692–702.

Pramanik, D., Dorst, N., Meesters, N., Spaans, M., Smets, E., Welten, M., et al. (2020) Evolution and development of three highly specialized floral structures of bee-pollinated *Phalaenopsis* species. *Evodevo* 11: 1–20.

Rao, X., Krom, N., Tang, Y., Widiez, T., Havkin-Frenkel, D., Belanger, F.C., et al. (2014) A deep transcriptomic analysis of pod development in the vanilla orchid (*Vanilla planifolia*). *BMC Genomics* 15: 1–12.

Raymond, O., Gouzy, J., Just, J., Badouin, H., Verdenaud, M., Lemainque, A., et al. (2018) The *Rosa* genome provides new insights into the domestication of modern roses. *Nat. Genet*. 50: 772–777.

Reposi, S.D., Gotelli, M.M. and Torretta, J.P. (2021) Anatomy and ultrastructure floral osmophores of *Catasetum fimbriatum* (Orchidaceae). *Protoplasma* 258: 1091–1102.

Robinson, M.D., McCarthy, D.J. and Smyth, G.K. (2009) edgeR: A Bioconductor package for differential expression analysis of digital gene expression data. *Bioinformatics* 26: 139–140.

Salzmann, C.C., Brown, A. and Schiestl, F.P. (2006) Floral scent emission and pollination syndromes: evolutionary changes from food to sexual deception. *Int. J. Plant Sci*. 167: 1197–1204.

Schiestl, F.P. (2010) The evolution of floral scent and insect chemical communication. *Ecol. Lett*. 13: 643–656.

Schiestl, F.P. and Johnson, S.D. (2013) Pollinator-mediated evolution of floral signals. *Trends Ecol. Evol*. 28: 307–315.

Schiestl, F.P. and Schlüter, P.M. (2009) Floral isolation, specialized pollination, and pollinator behavior in orchids. *Annu. Rev. Entomol*. 54: 425–446.

Schilmiller, A.L., Pichersky, E. and Last, R.L. (2012) Taming the hydra of specialized metabolism: how systems biology and comparative approaches are revolutionizing plant biochemistry. *Curr. Opin. Plant. Biol*. 15: 338–344.

Schlüter, P.M. and Schiestl, F.P. (2008) Molecular mechanisms of floral mimicry in orchids. *Trends Plant Sci*. 13: 228–235.

Schlüter, P.M., Xu, S., Gagliardini, V., Whittle, E., Shanklin, J., Grossniklaus, U., et al. (2011) Stearoyl-acyl carrier protein desaturases are associated with floral isolation in sexually deceptive orchids. *Proc. Natl. Acad. Sci. U. S. A*. 108: 5696–5701.

Schuurink, R. and Tissier, A. (2020) Glandular trichomes: micro-organs with model status?. *New Phytologist* 225: 2251–2266.

Schwacke, R., Ponce-Soto, G.Y., Krause, K., Bolger, A.M., Arsova, B., Hallab, A., et al. (2019) MapMan4: a refined protein classification and annotation framework applicable to multi-omics data analysis. *Molecular Plant* 12: 879–892.

Sedeek, K.E.E.M., Whittle, E., Guthörl, D., Grossniklaus, U., Shanklin, J. and Schlüter, P.M.M. (2016) Amino acid change in an orchid desaturase enables mimicry of the pollinator's sex pheromone. *Curr. Biol*. 26: 1505–1511.

Sedeek, K.E.M., Qi, W., Schauer, M.A., Gupta, A.K., Poveda, L., Xu, S., et al. (2013) Transcriptome and proteome data reveal candidate genes for pollinator attraction in sexually deceptive orchids. *PLoS One* 8: e64621.

Shan, X., Li, Y., Yang, S., Yang, Z., Qiu, M., Gao, R., et al. (2020) The spatio-temporal biosynthesis of floral flavonols is controlled by differential phylogenetic MYB regulators in *Freesia hybrida*. *New Phytologist* 228: 1864–1879.

Shang, J., Feng, D., Liu, H., Niu, L., Li, R., Li, Y., et al. (2024) Evolution of the biosynthetic pathways of terpene scent compounds in roses. *Curr. Biol*. 34: 3550–3563.e8.

Stökl, J., Brodmann, J., Dafni, A., Ayasse, M. and Hansson, B.S. (2011) Smells like aphids: orchid flowers mimic aphid alarm pheromones to attract hoverflies for pollination. *Proc. Biol. Sci*. 278: 1216–1222.

Sun, P., Schuurink, R.C., Caissard, J.C., Hugueney, P. and Baudino, S. (2016) My way: noncanonical biosynthesis pathways for plant volatiles. *Trends Plant Sci*. 21: 884–894.

Szenteczki, M.A., Godschalx, A.L., Gauthier, J., Gibernau, M., Rasmann, S. and Alvarez, N. (2022) Transcriptomic analysis of deceptively pollinated *Arum maculatum* (Araceae) reveals association between terpene synthase expression in floral trap chamber and species-specific pollinator attraction. *G3 Genes. Genomes Genet* 12: jkac175.

Szöcs, E., Stirling, T., Scott, E.R., Scharmüller, A. and Schäfer, R.B. (2020) Webchem: an R package to retrieve chemical information from the web. *J. Stat. Softw*. 93: 1–17.

Vignolini, S., Davey, M.P., Bateman, R.M., Rudall, P.J., Moyroud, E., Tratt, J., et al. (2012) The mirror crack'd: both pigment and structure contribute to the glossy blue appearance of the mirror orchid, *Ophrys speculum*. *New Phytologist* 196: 1038–1047.

Wang, Q.Q., Zhu, M.J., Yu, X., Bi, Y.Y., Zhou, Z., Chen, M.K., et al. (2021) Genome-wide identification and expression analysis of terpene synthase genes in *Cymbidium faberi*. *Front. Plant Sci*. 12: 751853.

Wang, Y., Xu, J. and Liu, A. (2022) Identification of the carotenoid cleavage dioxygenase genes and functional analysis reveal DoCCD1 is potentially involved in beta-ionone formation in *Dendrobium officinale*. *Front. Plant Sci*. 13: 1–14.

Waterhouse, R.M., Seppey, M., Simao, F.A., Manni, M., Ioannidis, P., Klioutchnikov, G., et al. (2018) BUSCO applications from quality assessments to gene prediction and phylogenomics. *Mol. Biol. Evol*. 35: 543–548.

Weston, P.H., Perkins, A.J., Indsto, J.O. and Clements, M.A. (2014) Phylogeny of Orchidaceae tribe Diurideae and its implications for the evolution of pollination systems. *In* R. Edens- Meier, & P. Bernhardt (Eds.), Darwin's Orchids: Then and Now. 91–154, The University of Chicago Press (Chicago, Illinois, U.S.A).

Williams, N.H. and Whitten, W.M. (1983) Orchid floral fragrances and male euglossine bees: methods and advances in the last sesquidecade. *Biol. Bull*. 164: 355–395.

Wong, D.C.J., Amarasinghe, R., Falara, V., Pichersky, E. and Peakall, R. (2019) Duplication and selection in β-ketoacyl-ACP synthase gene lineages in the sexually deceptive *Chiloglottis* (Orchidaceace). *Ann. Bot*. 123: 1053–1066.

Wong, D.C.J., Amarasinghe, R., Pichersky, E. and Peakall, R. (2018) Evidence for the involvement of fatty acid biosynthesis and degradation in the formation of insect sex pheromone-mimicking chiloglottones in sexually deceptive *Chiloglottis* orchids. *Front. Plant Sci*. 9: 389.

Wong, D.C.J., Amarasinghe, R., Rodriguez-Delgado, C., Eyles, R., Pichersky, E. and Peakall, R. (2017a) Tissue-specific floral transcriptome analysis of the sexually deceptive orchid *Chiloglottis trapeziformis* provides insights into the biosynthesis and regulation of its unique UV-B dependent floral volatile, chiloglottone 1. *Front. Plant Sci*. 8: 1260.

Wong, D.C.J. and Peakall, R. (2022) Orchid Phylotranscriptomics: the prospects of repurposing multi-tissue transcriptomes for phylogenetic analysis and beyond. *Front. Plant Sci*. 13: 910362.

Wong, D.C.J., Perkins, J. and Peakall, R. (2022a) Anthocyanin and flavonol glycoside metabolic pathways underpin floral color mimicry and contrast in a sexually deceptive orchid. *Front. Plant Sci*. 13: 860997.

Wong, D.C.J., Perkins, J. and Peakall, R. (2022b) Conserved pigment pathways underpin the dark insectiform floral structures of sexually deceptive *Chiloglottis* (Orchidaceae). *Front. Plant Sci*. 13: 976283.

Wong, D.C.J., Pichersky, E. and Peakall, R. (2017b) The biosynthesis of unusual floral volatiles and blends involved in orchid pollination by deception: current progress and future prospects. *Front. Plant Sci*. 8: 1955.

Wong, D.C.J., Pichersky, E. and Peakall, R. (2023) Many different flowers make a bouquet: lessons from specialized metabolite diversity in plant–pollinator interactions. *Curr. Opin. Plant. Biol*. 73: 102332.

Wong, D.C.J., Wang, Z., Perkins, J., Jin, X., Marsh, G.E., John, E.G. et al. (2024) The road less taken: dihydroflavonol 4-reductase inactivation and delphinidin anthocyanin loss underpins a natural intraspecific flower colour variation. *Mol. Ecol*. e17334..

Xiaohua, J., Dezhu, L., Zongxin, R. and Xiaoguo, X. (2012) A generalized deceptive pollination system of *Doritis pulcherrima* (Aeridinae: Orchidaceae) with non-reconfigured pollinaria. *BMC Plant Biol*. 12: 67.

Xu, H., Bohman, B., Wong, D.C.J., Rodriguez-Delgado, C., Scaffidi, A., Flematti, G.R., et al. (2017) Complex sexual deception in an orchid is achieved by co-opting two independent biosynthetic pathways for pollinator attraction. *Curr. Biol*. 27: 1867–1877.

Xu, Q., Wang, S., Hong, H. and Zhou, Y. (2019) Transcriptomic profiling of the flower scent biosynthesis pathway of *Cymbidium faberi* Rolfe and functional characterization of its jasmonic acid carboxyl methyltransferase gene. *BMC Genomics* 20: 1–14.

Yang, F.X., Gao, J., Wei, Y.L., Ren, R., Zhang, G.Q., Lu, C.Q., et al. (2021) The genome of *Cymbidium sinense* revealed the evolution of orchid traits. *Plant Biotechnol. J*. 19: 2501–2516.

Yang, H., Barros-Rios, J., Kourteva, G., Rao, X., Chen, F., Shen, H., et al. (2017) A re-evaluation of the final step of vanillin biosynthesis in the orchid *Vanilla planifolia*. *Phytochemistry* 139: 33–46.

Yeh, C.W., Zhong, H.Q., Ho, Y.F., Tian, Z.H. and Yeh, K.W. (2022) The diurnal emission of floral scent in *Oncidium* hybrid orchid is controlled by CIRCADIAN CLOCK ASSOCIATED 1 (CCA1) through the direct regulation on terpene synthase. *BMC Plant Biol*. 22: 1–12.

Yin, J., Zhang, C., Mirarab, S. and Schwartz, R. (2019) ASTRAL-MP: Scaling ASTRAL to very large datasets using randomization and parallelization. *Bioinformatics* 35: 3961–3969.

Zhang, C., Dai, Z., Ferrier, T., Orduña, L., Santiago, A., Peris, A., et al. (2023a) MYB24 orchestrates terpene and flavonol metabolism as light responses to anthocyanin depletion in variegated grape berries. *Plant Cell* 35: 1–28.

Zhang, D., Zhao, X.W., Li, Y.Y., Ke, S.J., Yin, W.L., Lan, S., et al. (2022) Advances and prospects of orchid research and industrialization. *Hortic. Res*. 9: uhac220.

Zhang, G., Hu, Y., Huang, M.Z., Huang, W.C., Liu, D.K., Zhang, D., et al. (2023b) Comprehensive phylogenetic analyses of Orchidaceae using nuclear genes and evolutionary insights into epiphytism. *J. Integr. Plant Biol*. 65: 1204–1225.

Zhang, G.Q., Liu, K.W., Li, Z., Lohaus, R., Hsiao, Y.Y., Niu, S.C., et al. (2017) The *Apostasia* genome and the evolution of orchids. *Nature* 549: 379–383.

Zhang, Y., Zhou, T., Dai, Z., Dai, X., Li, W., Cao, M., et al. (2020) Comparative transcriptomics provides insight into floral color polymorphism in a *Pleione limprichtii* orchid population. *Int. J. Mol. Sci*. 21: 247.

Zhang, Y., Zhang, Y., Zhang, A., Tian, Q., Yang, B., Wei, L., et al. (2025) Floral scent emission of Epiphyllum oxypetalum : discovery of its cytosol-localized geraniol biosynthesis. *Hortic. Res*.

Zhou, F. and Pichersky, E. (2020a) More is better: the diversity of terpene metabolism in plants. *Curr. Opin.Plant. Biol*. 55: 1–10.

Zhou, F. and Pichersky, E. (2020b) The complete functional characterisation of the terpene synthase family in tomato. *New Phytologist* 226: 1341–1360.